TML1 AND *TML2* SYNERGISTICALLY REGULATE NODULATION BUT NOT ARBUSCULAR MYCORRHIZA IN *MEDICAGO TRUNCATULA*

Diptee Chaulagain[1]*, Elise Schnabel[1]**, Erica Xinlei Lin[2], Rames Rosales Garcia[3,4], Rooksana E. Noorai[4], Lena Maria Müller[2]***, Julia A. Frugoli[1]

1. Department of Genetics & Biochemistry, Clemson University, Clemson, SC, USA
2. Department of Biology, University of Miami, Coral Gables, FL, USA
3. Department of Biological Sciences, Clemson University, Clemson, SC, USA
4. Clemson University Genomics and Bioinformatics Facility, Clemson University, Clemson, SC, USA

*currently at Department of Bioengineering, Clemson University, Clemson, SC, USA

**currently at Department of Plant and Environmental Sciences, Clemson University, Clemson, SC, USA

***currently at Plant Molecular and Cellular Biology Laboratory, Salk Institute for Biological Studies, La Jolla, CA, USA

Corresponding author: Julia Frugoli jfrugol@clemson.edu

154 Poole Agricultural Building

130 McGinty Court

Clemson, SC 29634-0318

Running title: TMLs autoregulate nodulation, not mycorrhization

Abstract

Two symbiotic processes, nodulation and arbuscular mycorrhiza, are primarily controlled by the plant's need for nitrogen (N) and phosphorus (P), respectively. Autoregulation of Nodulation (AON) and Autoregulation of Mycorrhization (AOM) share multiple components - plants that make too many nodules usually have higher arbuscule density. The protein TML (TOO MUCH LOVE) was shown to function in roots to maintain susceptibly to rhizobial infection under low N conditions and control nodule number through AON in *Lotus japonicus*. *M. truncatula* has two sequence homologs: *Mt*TML1 and *Mt*TML2. We report the generation of stable single and double mutants harboring multiple allelic variations in *MtTML1* and *MtTML2* using CRISPR-Cas9 targeted mutagenesis and screening of a transposon mutagenesis library. Plants containing single mutations in either gene produced twice the nodules of wild type plants whereas plants containing mutations in both genes displayed a synergistic effect, forming 20x more nodules and short roots compared to wild type plants. The synergistic effect on nodulation was maintained in the presence of 10mM nitrogen, but not observed in root length phenotypes. Examination of expression and heterozygote effects suggest genetic compensation may play a role in the observed synergy. However, plants with mutations in both *TMLs* had no detectable change in arbuscular mycorrhizal associations, suggesting that MtTMLs are specific to nodulation and nitrate signaling. The mutants created will be useful tools to dissect the mechanism of synergistic action of *Mt*TML1 and *Mt*TML2 in *M. truncatula* nodulation as well as the separation of AON from AOM.

Introduction

Since plants are sessile and require nutrients from the soil, they have developed strategies to maximize survival when the supply of nutrients is variable (Oldroyd and Leyser, 2020). Legume plants can grow in nitrogen (N) poor soil using an additional strategy beyond those of most dicots by establishing an endosymbiosis with Rhizobia bacteria which allows the N fixed from the atmosphere by the bacteria to be shared with the plant. Rhizobia are harbored in specialized root organs called nodules. The establishment of the legume root nodule symbiosis is tightly regulated, including species-specific signals from the rhizobia (lipochitin oligosaccharides) and internal plant signaling related to the carbon and N status of the plant. Obtaining N through symbiosis is energetically costly to the plant, resulting in regulation based on both available soil N, which appears to use common signals among most plants (Oldroyd and Leyser, 2020) and on already established nodulation, which uses a pathway called Autoregulation of Nodulation (AON) to control the number of nodules that form on a legume, reviewed in (Ferguson et al., 2019; Roy et al., 2020; Chaulagain and Frugoli, 2021).

The AON pathway negatively controls nodule number through systemic signal transduction and has been studied in many species; here we use *Medicago truncatula* nomenclature. Upon inoculation of *M. truncatula* with rhizobia, genes encoding the signaling peptides MtCLE12 and MtCLE13 are induced in the root (Mortier et al., 2010) through activation by NIN (Lin et al., 2018). MtCLE12 is post translationally glycosylated by the MtRDN1 enzyme before being translocated to the shoot (Kassaw et al., 2017). In the shoot, these CLE peptides are ligands for the leucine-rich receptor-like kinase (LRR-RLK) *M. truncatula* SUNN (SUPERNUMERARY NODULES) (Mortier et al., 2012). SUNN, which is the *M. truncatula* ortholog of Arabidopsis CLAVATA1, forms a putative complex with the pseudo kinase CORYNE

(CRN) and the receptor protein CLAVATA2 (CLV2) (Crook et al., 2016). MtCLE12,13/SUNN signaling in the shoot results in increased transport of cytokinin and decreased expression the of shoot-to-root signal miR2111 (Tsikou et al., 2018; Okuma et al., 2020; Okuma and Kawaguchi, 2021).

Reduced levels of miR2111 in roots correspond with increased expression of the *TML (TOO MUCH LOVE*) genes, which are F-box proteins that negatively regulate nodule number based on mutational analysis in *L. japonicus* which has only one *TML* gene and RNAi in *M. truncatula* which has two (Magori et al., 2009; Tsikou et al., 2018; Gautrat et al., 2019). The downregulating effect of miR2111 on *TML* transcripts is postulated based on the presence of predicted binding sites for miR2111 early in the *TML* gene and the observation that increasing miR2111 levels through overexpression in roots increases nodule number while decreasing the transcript levels of *TML* at five days post inoculation (dpi) (Gautrat et al., 2021). It has been suggested that other factors besides SUNN signaling contribute to this effect (Okuma and Kawaguchi, 2021), but at 5 dpi rhizobial inoculation decreases miR2111 expression in the shoots in an *MtSUNN* dependent manner resulting in a significant reduction in the nodule number from the hypernodulation phenotype. Data showing an miR2111 target mimic increases the *TML* transcript levels in a *sunn* mutant supports this mechanism (Gautrat et al., 2020).

The AON pathway appears to have at least two points of communication with the N acquisition pathway. NIN and NIN-like proteins, which activate the expression of CLE peptides, are linked to local N perception regulating nodulation (Nishida et al., 2018; Yan and Nambara, 2023). The *Mt*CLE35 peptide is locally upregulated in high N conditions and signals through SUNN and miR2111 to negatively regulate nodulation in the presence of N, with differential effects on the two *Mt*TMLs (Moreau et al., 2021).

Like nodulation, plant interactions with AM fungi are also controlled by autoregulation and plant nutrient status, including N and P. These signaling pathways share several, but not all, components and mechanisms with AON and N regulation of nodulation (Bashyal et al., 2023). In *M. truncatula*, autoregulation of mycorrhizal symbiosis (AOM) is mediated by the AM-induced peptide MtCLE53, which elicits a negative feedback loop that represses AM symbiosis in concert with the LRR-RLK SUNN (Müller et al., 2019; Karlo et al., 2020). Components of AOM are conserved beyond the legume clade: hyper-mycorrhizal mutants – characterized by elevated overall root length colonization and arbuscule numbers – in CLE peptides and orthologs of SUNN and CLV2 have been described not only in the legumes *M. truncatula*, soybean, pea, and *Lotus japonicus*, but also in the non-legumes *Brachypodium distachyon* and tomato (Morandi et al., 2000; Zakaria Solaiman et al., 2000; Meixner et al., 2005; Wang et al., 2018; Müller et al., 2019; Karlo et al., 2020; Wang et al., 2021).

AM symbiosis is also regulated by plant P and N status. Accumulating evidence suggests that P- and N-induced CLE peptides contribute to nutrient regulation of AM symbiosis; although our knowledge is still fragmented, at least some of the nutrient-regulated CLE peptides require the LRR-RLKs or other regulators of AOM and AON (Müller et al., 2019; Wang et al., 2021). Despite many similarities, AON, AOM, and N and P regulation of symbiosis are regulated by distinct CLE peptides. Emerging evidence from *M. truncatula* indicates that AON and AOM are at least partially symbiont-specific: Over-expression of the AON regulator *MtCLE13* roots does not affect AM symbiosis (Müller et al., 2019) and mutations in *MEDIATOR SUBUNIT 16A* suppress the hyper-nodulation but not the hyper-mycorrhizal phenotype of *sunn* (Chaulagain et al., 2023). The mechanisms of CLE perception by the LRR-RLK complex and signals downstream thereof, which may be responsible for symbiosis-specificity, remain largely elusive.

Thus far, *TML* is the only gene with a hypernodulation mutant phenotype reported to function downstream of the SUNN LRR-RLK in the AON pathway and was first described in *L. japonicus* (Magori et al., 2009). No gene downstream of SUNN with a hyper-mycorrhizal phenotype has been reported in the context of AOM. The *L. japonicus tml* mutant plants form ~8x more nodules spreading across larger area of root than wild type, a phenotype governed by root genotype (Magori et al., 2009). The gene encodes a protein containing a Nuclear Localization Signal (NLS), F-box domain, and kelch repeats (Takahara et al., 2013). *TML* action is proposed to be bifunctional in nodulation events: inhibiting nodule development after initiation of cortical cell division and inhibiting infection thread formation prior to rhizobial infection (Takahara et al., 2013). *M. truncatula* contains two sequence homologs of *LjTML*, *MtTML1* and *MtTML2.* Previous work demonstrated overexpression of *MtCLE12* and *MtCLE13* results in induction of *MtTML1* and *MtTML2* expression even in absence of rhizobia (Gautrat et al., 2019). In addition, MtCEP1 generated in response to low N, requires the MtCRA2 receptor to upregulate miR2111 expression in the shoots and hence lower the transcript level of both *MtTML*s to maintain root competence to nodulation (Gautrat et al., 2020).

The presence of kelch repeats and F-box domains in TML proteins suggest TMLs could bind to each other, as well as target other proteins for proteasomal degradation, however biochemical studies to identify such targets have not occurred yet. Genetic studies in *M. truncatula* have been hindered by of the lack of stable mutants and have been limited to RNAi experiments and measuring transcript levels (Gautrat et al., 2019; Gautrat et al., 2020). To understand the role of two TML proteins in nodulation, mutant analysis is critical. We obtained a mutant in *MtTML2*, *tml2-1*, from a *Tnt1* transposon insertion mutant library (Tadege et al., 2008) and generated stable single and double mutants harboring multiple allelic variations in *MtTML1* and *MtTML2* using

CRISPR-Cas9 targeted mutagenesis. Plants containing mutations in a single *MtTML* gene displayed approximately twice as many nodules as wild type plants, however plants containing mutations in both genes displayed a synergistic effect, with up to twentyfold more nodules than the wild type plants – six to ten-fold the nodules in either single mutant. A similar effect was observed for nitrate-insensitive nodulation: the single mutants were sensitive to nitrate and had wild type root length, but nodulation in the double mutant was unaffected by the presence of 10mM nitrate. By contrast, AM fungal root colonization was similar in wild-types and *tml* double mutants. Taken together with observations on gene expression and other phenotypes reported below, our findings demonstrate the requirement of both *MtTML1* and *MtTML2* in controlling nodule number through synergistic signaling in nodulation, but not AM symbiosis.

Results

The number of TML genes in a genome is not correlated with ability to nodulate or nodule meristem type

Since only one *TML* gene has been identified in *L. japonicus* (Magori et al., 2009) which forms determinate nodules, we wondered if having two copies of *TML*, like *M. truncatula* (Gautrat et al., 2019), was correlated with indeterminate nodulation, and how many copies appear in non-nodulating plants. Figure 1A displays a Maximum Likelihood tree for amino acid sequence homologs of LjTML identified by BLASTP in selected determinate and indeterminate nodule forming legumes, non-legume dicots and monocots. TML proteins from legumes clustered in a separate branch from non-legumes while single TMLs from the monocots rice, maize and sorghum clustered separately forming the tree root; these species have only ~40% amino acid sequence similarity with LjTML. In cases where non-legumes had two TML proteins, due to low similarity

to both TML1 and TML2, the first and second numbers are assigned randomly. The closest Arabidopsis protein, AtTML1/2, has only 51% amino acid sequence identity to LjTML but the *AtTML1* transcript is target of miR2111 (Hsieh et al., 2009; Pant et al., 2009) which also targets *LjTML* (Tsikou et al., 2018) and both *MtTMLs* (Gautrat et al., 2020). Among legumes, there is no correlation between *TML* gene number and nodule meristem type. The determinate nodule forming *L. japonicus* and *P. vulgaris* (common bean) have only one gene encoding a TML protein whereas determinate soybean has genes encoding three TML proteins. *GmTML1a* and *GmTML1b* are gene duplicates sharing 93.32% sequence identify and the encoded proteins cluster together in the phylogenetic tree, likely the result of the partially diploidized tetraploid soybean genome (Shultz et al., 2006). The TML2 protein sequences in legumes (*Gm*TML2, *Mt*TML2, *Ps*TML2 and *Tp*TML2) cluster together and separately from TML1 sequences, suggesting the two genes encoding TML proteins are not later duplications but evolved separately from a common ancestral duplication in these legumes.

Possible dimerization of TML proteins

Since there are two *TML*-like genes in multiple organisms and some of the phenotypes of the double mutants described below are not additive but synergistic, we explored the possibility of dimerization, using the AI protein structure prediction program AlphaFold. Since TML protein structure has not been predicted, we first ran AlphaFold (Jumper et al., 2021; Varadi et al., 2022) on each protein, generating the diagrams in Figure 1B and Supplemental Figure 1A and B). There is very little difference between the predicted structures of the two TML proteins, but the kelch repeats form the canonical "windmill" shape for protein: protein interactions, followed by the F-Box structure and a long flexible domain that might allow interactions with other proteins like transcription factors. The range of predicted local distance difference test (pLDDT) scores for

MtTML1 are 83.3 – 84.7 and for MtTML2 are 81.0 – 82.2. These scores are associated with confident predictions for protein structure (Varadi et al., 2022). We then used AlphaFold-Multimer (Evans et al., 2022; Zhu et al., 2023) to create "false proteins" containing a copy of each sequence connected by a linker. The range of values for the per-structure quality estimate score or interface predicted template modeling score (ipTM) were 0.238 – 0.395 which are below the stringent cutoff suggested by (O'Reilly et al., 2023) of > 0.85 to indicate a highly confident prediction. The highest ranked dimer, if formed (Figure 1D, Supplemental Figure 1 C) predicts MtTML1 and MtTML2 may dimerize by interactions of the kelch repeats while the F boxes and "tails" point outward.

Creation/identification of lines with mutations in MtTML genes

To explore the function of the two TML proteins in *M. truncatula*, we created and isolated mutant lines. The *tml2-1* allele was identified in a pool from the *Tnt1* insertional mutagenesis library from the Nobel Research Institute (Tadege et al., 2008) and isolated as a homozygous line (see Methods). Additional mutant alleles of *MtTML1* and *MtTML2,* as well as plants containing mutations in both genes, were generated by CRISPR-Cas9 mutagenesis of embryonic callus tissue followed by regeneration of whole plants in the R108 ecotype (see Methods). Multiple combinations of heterozygous and biallelic mutations were identified (Figure 2 and Supplemental Figure 2), including a single base deletion, a single base insertion, a deletion of a few base pairs in one or both targets of the gene, as well as a deletion of a larger fragment between the targets. The nature of the mutations for each allele used in this study is shown in Figure 2. Three homozygous lines were identified for *tml1* single mutants (*tml1-2*, *tml1-3*, and *tml1-4*), and *tml1/tml2* double mutants (*tml1-1 tml2-2*, *tml1-1 tml2-3* and *tml1-2 tml2-2*), and one for *tml2* single mutants (*tml2-2*). The *tml1-2* and *tml2-2* single mutants were obtained by segregation from the *tml1-2 tml2-2*

double mutant at backcross. In the five *tml1* and *tml2* alleles resulting in premature stop codons, the stop occurs prior to or early in the F-box coding region, so that any resulting truncated protein is not expected to contain the F-box, NLS, and kelch repeats (Figure 2). The binding sites for miR2111 in *MtTML1* and *MtTML2* start at 143bp and 134bp into the CDS respectively, and the binding site is lost only in the *tml1-4* mutant. (Supplemental Figure 2).

MtTML1 and MtTML2 single mutants have slightly increased nodule numbers while double mutants hypernodulate

The nodule number phenotypes of plants carrying three *tml11* alleles, two *tml2* alleles and three double mutant alleles were determined 10 days post inoculation (dpi) with *Sinorhizobium meliloti* RM41 and compared to wild type R108 plants and hypernodulating *sunn-5* plants described in (Crook et al., 2016; Nowak et al., 2019). In general, plants mutant in a single *TML* gene had more nodules than wild type plants, while plants with mutations in both *TML* genes had many more nodules and shorter roots than wild type plants (Figure 3A). All single mutant lines formed pink nodules similar in size to wild type plants (Figure 3B-F) whereas the double mutant plants formed small, fused nodules in a wider area of the root (Figure 3, G and H). Most nodules in the double mutants were white at 10 dpi, except for a few slightly pink nodules indicating leghemoglobin production. No obvious shoot phenotype was observed in any line.

All single and double mutants except *tml1-3* formed a significantly higher average number of nodules compared to wild type (Student's t-test with Bonferroni correction, $p<0.01$) and are displayed with confidence intervals (CI) (Figure 4A). The *tml1-3* plants had a mean of 9 nodules (95% CI [7,11]) compared to wild type (R108) plants with a mean of 5 nodules per plant (95% CI [3,7]) but failed the Bonferroni correction for multiple t-tests, however no there was no difference

in nodulation pattern (area or size of nodules) in *tml1-3* plants compared to other single mutant alleles. The *tml1-2* plants had a mean of 21 nodules per plant and all other single mutant alleles had means of 10 nodules per plant (Figure 4A insert). Examining all data together, the mean of nodules on plants harboring a mutation in a single *MtTML* gene was twice the mean of wild type plants.

Plants harboring mutations in both *MtTML* genes had mean nodule numbers 20-26 times higher than wild type plants. The mean nodule number of *tml1-1 tml2-3* plants was 134 (95% CI [105,162]), while the mean of *tml1-1 tml2-2* plants was 132 nodules (95% CI [92,171]), and that of *tml1-2 tml2-2* plants was 97 nodules (95% CI [83,110]) (Figure 4A). In contrast, the *sunn-5* mutant plants used as a comparison for hypernodulation had a mean of 57 nodules per plant (95% CI [42,72]).

Interestingly, the hypernodulating *tml* double mutant plants and the *sunn-5* plants, but not the *tml* single mutant plants, formed significantly shorter roots than the wild type plants in the presence of rhizobia (Student's t-test with Bonferroni correction, $p<0.001$) (Figure 4B). Because the number of nodules formed on a plant may affect root length, we examined plants grown in the absence of rhizobia in the same system with 10mM N. In the presence of sufficient N, all combinations of *tml* mutants tested had significantly shorter root lengths than wild type controls, with no statistical difference between any *tml* mutant and *sunn-5* plants. (Figure 4E), suggesting all mutations influence root length, but the effect of double mutation in root length is not additive.

Nitrate-insensitive nodulation occurs only in MtTML double mutants

As discussed in the introduction, *TML* genes have been implicated as downstream targets in both AON nodule number regulatory pathways and in CEP/CRA2 mineral N availability

response pathways. We wondered if the presence of two *TML* genes in *M. truncatula* might have resulted in a diversification of function between the two genes in regulating AON and nodulation competence in the presence of mineral N. To test this, we inoculated plants under the same conditions used in Figure 4A with the addition of 10mM N to the media. Comparison of mean nodule number from this experiment to that of Figure 4A showed that as expected, wild type plants reduced nodulation, and the same observation was made for plants containing a mutation in a single *TML* gene (Figure 4C). All *tml* single and double mutants had significantly more nodules than wild-type plants under these conditions (Figure 4C, D), however the same pattern was observed previously in the absence of nitrate (Figure 4A). When the change in mean nodule number with 10mM N is plotted as a percentage of the mean nodule numbers in the absence of N (Figure 4D), only plants carrying mutations in both *MtTML* genes did not reduce nodule numbers. Thus, nodulation was unaffected by N in the double mutant, but not in single mutants, suggesting both genes are required to control nodulation competence in the presence of mineral N.

MtTMLs differ in their spatiotemporal expression during nodule development

Using the ePlant resource for early nodulation (Schnabel et al., 2023) and past transcriptomics work in our lab (Schnabel et al., 2023) we examined the expression of the two *MtTML* genes in root segments during the first 72 hours responding to rhizobia (Figure 5). The genes are expressed in wild type plants at low levels at the 0 hr timepoint, which is 4-day old N starved plants in our experimental system, but expression rises in the vascular tissue for both genes at 12 and 24 hpi (Figure 5A). By 48 hpi when the nodules are beginning to form, *MtTML1* is expressed at a similar level throughout the vascular, cortical, and epidermal cells as well as the developing nodule, while *MtTML2* increases to a higher level in the vascular and inner cortical

cells at the xylem poles and does not increase in the nodule. By the time the nodule has organized and begun to emerge at 72 hpi, this difference in pattern is reinforced, with *MtTML1* highly expressed in the nodule and *MtTML2* expressed in the nodule at the same low level as in tissues of uninoculated plants. Following expression in undissected root segments over time (Figure 5B), both genes are induced by rhizobia in wild type (green line versus blue line) over 72 hours, as well as in the hypernodulation mutant *sunn-4* (orange versus gray line). However, as reported in (Schnabel et al., 2023) *TML1* expression does not begin to decrease over this time frame in the *sunn-4* mutant, while *TML2* does. Examined at the level of single cell RNASeq over a time course of combined experiments harvested at time points at 0, 48 and 96 hpi, a tissue heatmap of the combined transcriptomics data of individual cells shows both *TML* genes are expressed maximally in the vascular bundle cells and moderately in the pericycle cells, but only *TML1* is expressed in cells identified as nodule and cortex (Figure 5C). The data in C support the data in A and B, while adding more detail. Taken together, MtTML1 and MtTML2 have a spatiotemporal effect on nodulation; *MtTMl1* has higher expression in cortical cells and nodules whereas *MtTML2* is expressed mainly in the vasculature.

TML1 mutants show evidence of transcriptional adaptation

Genetic compensation can occur by several mechanisms but transcriptional adaptation, in which degradation of the mutant mRNA transcript triggers increased expression of a paralog or family member (El-Brolosy et al., 2019), is straightforward to test. Using Real Time Quantitative PCR, we measured expression of one wild type *MtTML* gene when the other *MtTML* was mutated. In the roots of wild type R108 and plants containing either a *tml2* or *tml1*mutant transcript, there is no statistical difference in expression of the wild type *TML* message at 0 hpi, and all plants

showed statistical increases in expression of the examined transcript from the uninoculated level (0 hpi) compared to 72 hpi ($p<0.05$) (Figure5 D, E). In *tml2* mutants (Figure 5D), the expression level of *MtTML1* at 72 hpi is statistically equivalent to wild type at 72 hpi, showing no evidence of genetic compensation. However, in *tml1-4* mutants (Figure 5E) the expression level of *MtTML2* is increased from that of wild type at 72 hpi ($p<0.05$) suggesting that the loss of a functional copy of *MtTML1* increases the expression of *MtTML2*, but not vice versa. In wild type plants, the fold changes of *TML1* at 72 hpi are half that of *TML2*, which could make differences in *TML1* expression significance harder to detect.

Phenotypic effects of heterozygosity appear in segregation of double TML mutants

Following the observation that the observed increase in expression of the wild type *TML2* gene in a plant containing a mutation in *TML1* does not rescue the nodule number phenotype in the *tml2* mutant, we wondered if there could be a small effect. While an intermediate nodule number for plants heterozygous for a *tml* mutation might be difficult to detect given the given the small size of the effect on nodule number of a single mutation, the magnitude of the phenotype of double mutants could allow a nodule number difference to be detectable when plants are homozygous for one mutant allele and heterozygous for the other.

To investigate we examined two populations of progeny obtained from selfing plants homozygous for one *tml* mutation and heterozygous for the other; a discrete recessive phenotype should segregate nodule number phenotypes in a 3:1 Mendelian ratio. Instead, both populations segregated a broad distribution of nodule number phenotypes (Figure 6A). To test our hypothesis that this distribution of phenotypes is due to changes in the inheritance of the segregating wild type copy, we used the progeny of plants homozygous for *tml2-2* and segregating *tml1-2*, because *tml1*

mutants showed genetic compensation and mutation in *tml1-2* generates a size polymorphism useful for distinguishing wild type from mutant alleles by PCR. We tested 89% of the population with fewer than 80 nodules (65% of the total population) and observed a difference in mean nodule number between plants wild type for the segregating allele (24.2 nodules) and plants heterozygous for the segregating allele (43.8 nodules) versus plants homozygous for both mutant alleles (106.3 nodules). (Figure 6B). The data suggest the expression levels of both genes contribute to the nodule number phenotype.

tml double mutants do not affect arbuscular mycorrhizal symbiosis

Many AON mutants also have hyper-mycorrhizal phenotypes, since they share common pathway components, and *miRNA2111* is induced upon phosphate starvation even in Arabidopsis which does not nodulate (Hsieh et al., 2009). Expecting an increase in AM fungal root colonization, we tested the double *tml1-1,2-2* mutants for a mycorrhizal phenotype with the AM fungus *Rhizophagus irregularis*. Surprisingly, no difference from wild type was observed both in terms of overall root length colonization or arbuscule density under our growth conditions (Figure 7), suggesting *MtTML1* and *MtTML2* are specific to nodulation signaling but play no substantial role in AM symbiosis.

Discussion

While the *TML* gene was first identified and investigated in *L. japonicus* (Ishikawa et al., 2008; Yokota et al., 2009 (Magori et al., 2009) the legumes and most dicots examined contain two distinct copies of a TML-like gene, with tomato and *L. japonicus* as outliers (Takahara et al., 2013).

Based on our ability to only identify one copy in the monocots we analyzed, we suspect an ancestral duplication early in the dicot lineage, followed by the loss of a copy in *L. japonicus* and tomato. As is common for many genes in soybean, the *G. max* genome contains two copies of *TML1*, which we have labeled a and b (Figure 1A). Since monocots and dicots diverged approximately 200 million years ago (Wolfe et al., 1989), enough time has passed for the genes to have adopted divergent functions, but this work suggests any divergence is complex, and the genes have evolved to give synergistic effects in some of the phenotypes tested and none in others.

Given the moderate effect of RNAi against the *M. truncatula TMLs* on nodulation phenotypes (Gautrat et al., 2019), we expected the strong genetic mutants created in this study (stop codons early in the gene) to have a larger effect on phenotype than observed. However, multiple CRISPR mutations and a *Tnt1* insertion, which all are predicted to result in highly truncated proteins if translated, had small effects, with only twice the number of nodules as wild type (Figure 4A). While the *tml1-3* allele was not statistically different from wild type, the smaller number of plants available to test phenotype (N=6) may have contributed to the lack of statistical significance, and this allele was not used in the rest of our analysis. In sharp contrast, mutation in the single copy of *TML* in *L. japonicus* results in eight times more nodules than wild type (Magori et al., 2009). When both copies of *TML* were disrupted in *M. truncatula,* the nodule number phenotype was logarithmically increased, exceeding that observed for *sunn* mutants (Figure 4A) and for the *L. japonicus tml* mutant (Magori et al., 2009). In our aeroponics system (Cai et al., 2023), all plants encounter rhizobia at the same time, leading to a distinct zone of nodulation even in AON mutants such as *sunn* and *rdn1* (Schnabel et al., 2005; Schnabel et al., 2011). Interestingly, while we observed the same effect in single *tml* mutants, the double mutants nodulated along the entire root (Figure 3) suggesting that competence to nodulate may be more than just on/off switch

(Laffont and Frugier, 2023) and other characteristics such as the extent of the nodulation zone or the speed of nodule development could be regulated by a signal dependent on both TML proteins.

(Nishida et al., 2020) observed a wild-type response to nodulation in the presence of N (decreased nodule number) in the *L. janponicus tml* mutant, suggesting the gene is not involved in limiting competence to nodulate in the presence of N in *L. japonicus*. We observed a similar effect in our single mutants, however loss of both *TML* genes resulted in N blind nodulation-there was no difference in nodule number on double mutants between the low and high N conditions (Figure 4C, D). Again, this suggests that competence to nodulate in the presence of N is regulated by a signal dependent on both TMLs, or that compensation occurs in single mutants.

A signal dependent on both TMLs was not observed in analyzing root length phenotypes. AON mutants have shorter roots than wild type plants when they nodulate, and in *sunn* and *rdn1* mutants, root length is shorter than wild type even in the absence of rhizobia (Schnabel et al., 2005; Schnabel et al., 2011). When inoculated with rhizobia the AON control *sunn-5* and the *tml* double mutants had shorter roots than wild type, but the single *tml* mutants did not (Fig 4B). In the absence of rhizobia, both single and double *tml* mutants had a root length phenotype significantly different from wild type and statistically the same as *sunn-5*, but not different between single and double mutants (Figure 4E). This suggests that the root length phenotype observed when nodulating is due to the extreme nodulation of the double mutant, but the observation also suggests mutation of any *TML* affects a signaling pathway outside the SUNN AON pathway that influences root length, likely N effects on root growth. Because the same effect was observed in all mutant combinations without rhizobia, the data imply root length is regulated by a signal dependent on the presence of each TML, without genetic compensation.

The observation of transcriptional adaptation in *tml1* mutants which increase the expression of the *TML2* gene during nodulation (Figure 5) strongly suggests some overlap in function between the two genes. The loss of *TML1* (which is expressed in the nodules at 72 hpi-Figure 5A) can be partially compensated for by increased expression of *TML2*, which is normally not expressed in the nodules. However, identification of a weak phenotype in *TML* single mutants also means that the two genes are not completely redundant. As noted in the description of the results, because the fold change in *TML1* expression is much smaller than that of *TML2,* genetic compensation for *TML1* in *tml2* mutants could exist but be too small for a significant change in expression. However, even if genetic compensation did not occur, an overlap of function explains the small effect on nodule number. Additionally, the differences in mean nodule number for *tml1-2 TML1* heterozygotes segregating in a *tml2-2* background versus plants carrying a wild type allele in the same background and the observation of a similar distribution of nodule number in *tml2-2 TML2* heterozygotes segregating in a *tml1-2* background (Figure 6, Supplemental Figure 3) indicate that the level of wild type *TML* message (*TML1* + *TML2*) affects the number of nodules formed. Intriguingly, the synergistic effect of loss of both genes on nodule number and N sensitive nodulation competence but not root length in adequate N is evidence that both genes are involved in nodulation, nitrate sensing and root length, but suggests different modes of action or in different signaling pathways for the phenotypes.

Synergistic gene interaction can have multiple causes (Pérez-Pérez et al., 2009). The single and double mutant alleles in this analysis contain premature stop codons (Figure 2) resulting at best in a truncated protein without any functional domains. The prediction of complete loss of function (null) mutations thus rules out that the synergistic phenotype is the result of hypomorphic alleles. Synergy can also be the result of mutations in in two unrelated genes acting in parallel

pathway that converge at a node or completely or partially redundant paralogous genes functioning in the same step of a linear pathway or mutation. The *TML* genes are not unrelated, ruling out the first cause. The *MtTML1* and *MtTML2* genes cannot be completely redundant genes acting in same spatiotemporal step; if so the effect of mutation in one *MtTML* gene should be completely complemented by the presence of a wild type copy of the other *TML* gene; hence there would be no nodulation phenotype in plants carrying mutation in only one gene or in the heterozygotes and this is not observed. Partial redundancy of two genes functioning in the same step can be a result of a differential expression pattern in which genes perform same function in different cellular locations or in different tissue types. Tissue expression data from wild type (Figure 5A) shows both *MtTML1* and *MtTML2* transcripts increasing in wild type responding to rhizobia over 72 hpi, but there are small differences in both tissues and levels of expression of the *MtTML* genes at 72 hpi. Both *MtTML1* and *MtTML2* are detected at 24 hpi in the vasculature (pericycle), however *MtTML1* is expressed in the nodules and cortex at 48 and 72 hpi as well, while *MtTML2* expression remains vascular. The result is different transcript levels in different tissues, suggesting a tissue specific role for at least *MtTML1*. Since the root segment expression pattern (Figure 5B) also shows a difference in temporal expression pattern between *MtTML1* and *MtTML2*, this may indicate similar functions but a different spatial role for *TML1*.

Finally, synergy can be observed when the products of two genes interact in a multimeric protein complex; mutation of one component leads to fewer monomers resulting in fewer functional protein complex in a dose-dependent manner. One explanation for both the individual phenotypes and the synergy observed is that the two proteins form homo or heterodimers as part of their downstream signaling. The prediction of a possible heterodimer between TML1 and TML2 (Figure 1) would explain some of the synergistic effects observed, but the confidence score for the

best predicted dimer is not within the stringent cutoff suggested in the literature (O'Reilly et al., 2023). While the score does not indicate this structure is impossible, it is unlikely, and any interaction would need to be confirmed biochemically. It is also not possible to computationally rule out higher order multimers of single TML proteins. Most likely, the two proteins might function together bound to a third target, such as a promoter, a transcription factor, or to provide the localization signal to bring a factor into the nucleus.

Given that TML regulation of AON is predicted to result from destruction of the mRNA during nodulation signaling by miR2111, it is likely that the synergy comes from a dosage dependence of the wild-type message combined with genetic compensation. The lower transcript levels of both *MtTML1* and *MtTML2* in roots under low N conditions is correlated with root competence to nodulation (0 hpi in Figure 5) whereas higher transcript levels of both genes is correlated with inhibition of nodulation after rhizobial inoculation later in time (Gautrat et al., 2020) (72 hpi in Figure 5). It is not clear whether both MtTML proteins use the same signal transduction pathway to maintain N root competence to nodulation and in AON, but the effects of the mutations are similar.

A key factor in the AON model is miR2111 produced in the shoot and transported to the root (Okuma and Kawaguchi, 2021; Bashyal et al., 2023). Multiple genes encode miR2111, which is predicted to bind to *TML* RNA and decrease RNA levels versus preventing transcription. (Gautrat et al., 2020). When N is abundant, *MtCLE35* is induced in the roots and represses miR2111 in the shoots and roots, resulting in low abundance of miR2111 in the roots and thus higher levels of *TML* message (Tsikou et al., 2018; Gautrat et al., 2020; Moreau et al., 2021). Low N is signaled through systemic CEP7/CRA2 peptide/receptor signaling and reduction of systemic MtCLE35/SUNN peptide/receptor signaling. Both signals are transduced through miR2111 levels

dropping and *TML* message levels rising, signaling competence to nodulate (Moreau et al., 2021; Laffont and Frugier, 2023). When competent plants begin to nodulate, *TML* levels continue to rise as nodulation begins along with CLE13/SUNN signaling (Schnabel et al., 2023) and fall as nodulation proceeds and miR2111 levels rise, a result of the CLE13/SUNN signal AON feedback.

The current AON model is highly simplified, involving signal transduction in both space and time based on evidence gathered by multiple groups in multiple systems and species. What appear to be differences in *MtTML* expression results between our work and others can explained by differences in timing and set up between experiments - the decreased *MtTML* expression data in (Gautrat et al., 2020) was collected at 5 dpi in whole roots on plates versus the increase of *MtTML1* in (Schnabel et al., 2023) at 3 dpi in nodulating segments of roots in an aeroponic chamber. Additionally, we do not know the half-life of the MtTML proteins, which would affect the length of time between detecting decreased mRNA and the action of the MtTML proteins in halting nodulation; split root analysis suggests the AON systemic signal has an effect on nodule number within 72 hpi in *M. truncatula* (Kassaw et al., 2015) but no decreased *TML* expression is detected during this time. Our results in general support the position of TML in the AON model, but also provide evidence that the functions of the individual *MtTML* genes are not redundant.

AON and AOM share multiple common components, including common LRR-RLKs that perceive distinct CLE peptides specific to nodulation and AM symbiosis, respectively (Roy and Müller, 2022). When legumes are inoculated with rhizobia and AM fungi, the two symbioses influence each other (Catford et al., 2003), potentially by competing for carbon. However, we previously reported that the AON regulator MtCLE13 does not influence AM symbiosis, suggesting AON and AOM have symbiosis-specific signaling outcomes (Müller et al., 2019). Because the distinct CLE signals mediating AON, AOM, and P and N regulation of nodulation

and AM symbiosis, converge at the same LRR-RLK SUNN but result in at least partially distinct outcomes (Figure 8), it appears plants can distinguish between the signals. Our results demonstrate that *M. truncatula TML1* and *TML2* are specific components of AON signaling and do not play a role in AOM signaling, at least under our growth conditions. This suggests that symbiosis-specific signaling must occur upstream of TML, potentially during CLE perception (e.g., through assembly of CLE-specific receptor complexes) and/or the activation of CLE-specific downstream signaling cascades (Bashyal et al., 2023). Our knowledge on receptor complex components regulating AM symbiosis is fragmented across species and signaling components downstream of CLE perception remain completely elusive. Because legumes can engage in nodulation and AM symbiosis, they constitute excellent models to decipher signaling specificity of closely related symbiotic CLE pathways. It will be interesting to determine if known signaling components mediating AON in legumes (e.g., CLV2, CRN, KLV, miR2111) also play a role during AOM in legumes.

During nodulation symbiosis, miR2111 is also regulated by N-starvation-induced CEP peptides that signal through the RLK CRA2 (Laffont et al., 2019; Laffont et al., 2020; Ivanovici, 2021; Ivanovici et al., 2023; Lepetit and Brouquisse, 2023). It is unknown if CRA2, CEP peptides, or miR211 also regulate AM symbiosis. Because TML has also been implicated in N regulation of nodulation in *L. japonicus* and *M. truncatula* (Tsikou et al., 2018; Gautrat et al., 2020; Gautrat et al., 2021; Okuma and Kawaguchi, 2021; Tiwari et al., 2021), it is possible that TML may play a minor role in N regulation of AM as well. In tomato, the phenotypes of hyper-mycorrhizal mutants were shown to be dependent on N conditions (Wang et al., 2021). With our experiments, we cannot rule out a minor role of MtTML1 and MtTML2 in N regulation of AM symbiosis in *M. truncatula*. However, based on our experience with other hyper-mycorrhizal mutants in the same conditions (Müller et al., 2019; Chaulagain et al., 2023) we should have observed at least small

AM colonization differences between *tml1,2* double mutants and wild-type controls if *TML* contribution to AM symbiosis regulation were substantial. Because the protein targets of TML are unknown, it is possible that those targets are nodulation specific.

This study uncovered the non-redundant role of MtTML1 and MtTML2 in AON while excluding a role in AOM (Figure 8). This opens a new avenue for definitive additional experiments in *M. truncatula* to refine and fill in gaps in the model with the *MtTML* mutants we have created. It is unknown how *SUNN* signaling results in changes in miR2111 expression in the shoot or whether the destruction of *TML* RNA by miR2111 binding in the root affects further *TML* expression. It is unknown how the TML proteins exert their effects and through what other proteins (though the presence of nuclear localization signals might suggest interaction with transcription factors). It is possible there are regulatory steps that involve loading and unloading in the vasculature or import to the nucleus that involve other proteins TML reacts with. Knowing SUNN signaling in AOM does not include TMLs, at least under the conditions investigated, opens the door to new investigations on the regulation of AM symbiosis. The mutants described here will allow these and other important questions to be investigated.

Methods

Plant Growth Conditions

Seeds were germinated as described previously (Schnabel et al., 2010). Briefly, seeds were scarified using concentrated sulfuric acid, imbibed in water, vernalized at 4°C for 2 days and allowed to germinate overnight at room temperature in dark. One day old seedlings were placed in an aeroponic chamber and grown at 21°C-25°C; 14h/10h light/dark cycle and inoculated as described in (Cai et al., 2023). To determine nodulation phenotypes no N was included in the

media (unless otherwise specified) and plants were inoculated *Sinorhizobium meliloti* RM41 (Putnoky et al., 1990) four days post germination as indicated. Nodule count and root length measurements were performed 10 days post inoculation (dpi), unless otherwise noted. For seed collection and genetic crosses, plants were grown in a greenhouse with supplemental light on a 14h/10h light/dark cycle at 21°C-25°C. For mycorrhizal assays, seed germination and inoculation with *Rhizophagus irregularis* was performed as previously described (Chaulagain et al., 2023). In brief, 3-day old seedlings were planted in Cone-tainers SC10R (Steuwe and Sons) and placed in a growth chamber with 16h/8h light/dark cycle at 22°C-24°C and 40% humidity. The growth mixture was 50% play sand (Quickrete) and 50% fine vermiculite (Ferry-Morse). All substrate components were washed in distilled water and autoclaved for 55 minutes before use. For colonization with *R. irregularis*, 250 spores (Premiertech, Canada) were placed 5 cm below the surface in a layer of fine sand. All plants were treated twice a week with 15ml of half-strength, low Pi Hoagland's fertilizer (20µM phosphate) to aid in symbiosis initiation. Plants were harvested 29 days post planting.

Tnt1 mutant screening and verification of insert

Tnt1 insertion lines created by *Tnt1* mutagenesis of the R108 ecotype (Tadege et al., 2008) were screened electronically for insertions in *MtTML* genes. While no *MtTML1* insertion lines were identified, a pool of plants containing a mutation in the *MtTML2* gene in *M. truncatula* (NF0679) Nobel Foundation Medicago Mutant Database now located at https://medicagomutant.dasnr.okstate.edu/mutant/index.php. Seeds from the NF0679 pool were grown in the greenhouse and a line containing the insertion in the second exon was identified by PCR using primers from Supplemental Table 2. The primer set 2189/2190 amplifies a 1.15 kb

product from wild type DNA and the primer set 2189/1925 amplifies a product of 979 bp only when *Tnt1* insert is present. The line was selfed to yield homozygotes, which were then backcrossed to the R108 wild type and re-isolated. The amplicons generated by primers 2189/1925 and 2690/3227 were sequenced to determine the exact position of the *Tnt1* insertion in relation to the gene. This line is called *tml2-1*.

Constructs for CRISPR-Cas9 mutagenesis

Multi target constructs were designed for *MtTML1* alone and to target both *MtTML* genes in the same plant (Supplemental Figure 1). Two target sites per gene were chosen following the target selection criteria (Ma and Liu, 2016) Unique sites were selected to avoid off-target mutagenesis by comparison to the *M. truncatula* genome MtV4.0 (Tang et al., 2014). The binary vector pDIRECT_23C (Čermák et al., 2017) (Addgene) was used as Cas9 containing vector. The target and gRNA were cloned into the pDIRECT_23C vector and the finished construct created using Golden Gate assembly (Engler et al., 2008; Engler et al., 2009) following the protocol in (Čermák et al., 2017). The resulting vectors pDIRECT_23C+MtTML1 (containing two targets for *MtTML1*) and pDIRECT_23C+MtTML1/2 (containing two targets each for *MtTML1* and *MtTML2)* were then verified by sequencing. A verified clone in *E. coli* (Zymo 10B, Zymo Research) was used as plasmid source to move each construct into *Agrobacterium tumefaciens* EHA105 (Hood et al., 1993) for use in plant transformation.

Generation of transgenic plants using CRISPR-Cas9 mutagenesis

To obtain alleles of *MtTML1*, additional alleles of *MtTML2* and plants containing mutations in both genes, CRISPR-Cas9 mutagenesis of embryonic callus tissue followed by regeneration of

whole plants was performed in the R108 ecotype. Each construct was introduced with *Agrobacterium* mediated transformation into root segments of 4-7 day old R108 seedlings and taken through callus and tissue culture following the protocol 2A of (Wen et al., 2019) with the following modifications for selection and rooting: the selection of phosphinothricin (ppt) resistant callus used 2mg/L ppt in the media and 2mg/L NAA was used in RCTM6 medium for rooting. All plants originating from a callus were considered one independent line. The three most developed plants at the rooting medium stage for each line per callus were transferred into soil for acclimatization and grown to collect seeds.

Transgenic verification, genotyping, and segregation of targeted mutagenesis in T1 generation

All T0 lines generated from tissue culture were screened by PCR for the presence of the transgene using Cas9 specific primers (primers 3081/3082; Supplemental Table 2), and lines testing positive were then screened by PCR for deletions using gene specific primers (3065/3066 for *MtTML1*; 3148/3149 for *MtTML2*; Supplemental Table 2). Deletion was confirmed by size difference of an amplicon after gel electrophoresis. All the amplicons were sequenced using the same primers as for the PCR to determine the exact mutations.

All T0 lines containing mutations were allowed to set seeds. To generate a *tml1* homozygous mutant, a T0 line containing a 107 bp deletion allele and a single nucleotide insertion allele was used. The T1 generation was screened for plants homozygous for a single allele by PCR. Simply, the deletion allele was identified by a size difference in a gel and the insertion allele using *BstXI* digestion, as the insertion creates a natural CAPS marker (Primers in Supplemental Table 2). All amplicons were sequenced to confirm homozygosity and sequence. The alleles were named *tml1-3* (insertion) and *tml1-4* (deletion) (Figure 2).

To generate the tml*1/tml2* double mutant transgenic line, a T0 line carrying two mutant alleles for each gene was used. Homozygous double mutants with allelic combinations of: *tml1-1 tml2-2*, *tml1-1 tml2-3* and *tml1-2 tml2-2* were identified. The segregation of alleles in T1 was tested using the size difference in gel or CAPS marker or sequencing for the single base pair insertion; *tml1-1* by CAPS marker (HaeIII digestion), *tml1-2* by size difference (contains 333bp deletion), *tml2-2* and *tml2-3* by sequencing (Supplemental Table 2 for primers). All the homozygous plants were PCR tested for Cas9 segregation as well. The homozygous double mutant progeny (*tml1-2 tml2-2*) had no detectable Cas9. All alleles except *tml1-3, tml1-4* and *tml1-1 tml2-3* were backcrossed once to R018 and do not have detectable Cas9 when tested by PCR amplification.

Real Time PCR Analysis of MtTML in mutant plants

RNA was extracted from roots of mutants and R108 (wild type -WT) harvested at 10 days post inoculation with RM41. Root tissue was frozen at -80°C until RNA extraction. Root tissue from six plant pooled together for each genotype was ground in liquid nitrogen and 100mg of tissue was used for RNA extraction. RNA was extracted using TRIzol® Reagent (Life Technologies, USA) followed by DNase digestion using RQ1 RNase free DNase (PROMEGA, USA) according to manufacturer's instructions. cDNA was synthesized using iScript™ Reverse Transcriptase (BIO-RAD, USA) according to manufacturer's instructions. Real-time qPCR was performed in 10 µl reactions in an iQ5 instrument (Bio-Rad, CA, USA) using iTaq™ Universal SYBR® Green Supermix (Bio-Rad, CA, USA) and a 400 nM final concentration of each primer from (Supplemental Table 2) Each reaction was run in three technical and three biological replicates. Relative expression levels of genes were assayed using the Pfaffl method (Pfaffl 2001) relative to a previously validated housekeeping reference gene phosphatidylinositol 3- and 4-

kinase belonging to the ubiquitin family (PI4K; Medtr3g091400 in MtV4.0, MtrunA17Chr3g0126781 in MtrunA17r5.0-ANR) (Kakar et al., 2008). Data from the three biological replicates were used to estimate the mean and standard error.

DNA isolation

Leaf presses were made by pressing a leaflet of each plant to a Plant Card (Whatman™, GE Healthcare UK Limited, UK) for long term storage. A 1.2 mm diameter piece of Plant Card was excised and washed with Whatman™ FTA Purification Reagent (GE Healthcare UK Limited, UK) followed by TE-1 buffer according to the manufacturer's instructions and directly used in PCR. DNA from R108 wild type, used multiple times, was isolated using the DNeasy Plant Mini Kit (Qiagen, Hilden, Germany) as per the manufacturer's instruction.

PCR conditions

All amplification except for use in cloning was performed with GoTaq® G2 DNA Polymerase (Promega Corporation, Madison, USA) following manufacturer's instructions and buffers. Standard PCR conditions used were: 2 min at 95°C, 35 cycles (10 s at 95°C, 15 s at gene specific annealing temperature, 30 s/Kb at 72°C), 5 min at 95°C. When using leaf press as DNA template for amplification, cycles were increased from 35 to 40. The gene specific annealing temperature was 55°C except as noted for primer pairs 3148/3149 (58°C), 3182/3183 (52°C), and 2493/2494 (56°C). Annealing temperatures were predicted using the 'Tm Calculator' tool available at https://www.thermofisher.com/. Amplification of inserts for cloning were performed with iProof™ High-Fidelity DNA Polymerase (Bio-Rad Laboratories, USA) and buffers according to the manufacturer's instructions.

Imaging

The nodule images in Figure 3 were taken using the Leica Microsystems THUNDER Imager Model Organism with the attached DMC4500 color camera. For visualization of AM fungal structures (Figure 7), colonized roots were cleared in 20% KOH (w/v) at 65°C for two days. Then, they were rinsed three times with ddH2O for at least one day until the roots appeared white, and the pH was neutralized overnight using 1x PBS. Cleared roots were stained in Alexa Fluor® 488 wheat germ agglutinin (WGA)-PBS solution so the final concentration of WGA was 0.2ug/ml. AMF colonization was quantified using the magnified intersections method with a gridded square petri dish (McGonigle et al., 1990). Quantification of arbuscule density (defined as number of arbuscules per mm of colonized root) was performed as previously described (Chaulagain et al., 2023). Images were captured with a Leica Thunder Imager and analyzed using Fiji.

Computational and Statistical analysis

The tree in Figure 1 was generated with (MEGA11 (Tamura et al., 2021)) using the maximum likelihood method and tested using Bootstrap for 1000 replicates. Student's t-test was used to analyze the difference in means in Figure 4 with Bonferroni correction to adjust for multiple t-tests. JMP software was used to create plots in Figures 4 and Confidence Intervals were determined by the software. AlphaFold v2.3.1 (Jumper et al., 2021; Varadi et al., 2022) was run in CPU mode and default settings including setting the maximum template release date to 2023-10-01 on the protein sequences for MtTML1 and MtTML2 separately. An input file combining both protein sequences was run with AlphaFold in multimer mode (Ghani et al., 2021; Evans et al., 2022; Zhu et al., 2023), CPU mode, and default settings including a maximum template release date of 2023-

10-01. Values for pLDDT or ipTM scores were taken from the corresponding 'ranking_debug.json' output file. Each instance of AlphaFold was run on a high memory compute node on the Clemson University Palmetto Cluster. The highest ranked model for each analysis was visualized using the Mol* 3D viewer (https://www.rcsb.org/3d-view).

Acknowledgement & Funding

We acknowledge Clemson Light Imaging Facility and Dr. Terri Bruce, Rhonda Powell and J. Conrad Epps for training and assistance with the Leica THUNDER Imager equipment use. Much of the computation was done on Clemson University's Palmetto Cluster. We acknowledge Hemani Patel, an undergraduate mentored by Diptee Chaulagain, for the PCR work on segregating single mutants from the double mutant allele. We thank Dr. Li Wen for teaching *M. truncatula* crossing to DC and Dr. Yuanling Chen for tissue culture tips and troubleshooting. This work was supported by NSF 1733470 to JF and USDA-NIFA 2022−67013−36881 to LMM. R.E.N. and computational infrastructure at the Clemson University Genomics and Bioinformatics Facility are supported by two Institutional Development Awards (IDeA) from the National Institute of General Medical Sciences of the National Institutes of Health under grant numbers P20GM146584 and P20GM139767.

Authorship contributions

D.C. designed the research, performed research, analyzed data

E.S. designed the research, performed research

E.L. performed research

R.E.N. analyzed data

R.G. performed research, contributed new computational tools; analyzed data

L.M.M. designed the research, performed research; analyzed data

J.F. designed the research, performed research; analyzed data

All authors contributed to drafting the work or revising it critically for important intellectual content.

Figure Legends:

Figure 1: Phylogenetic analysis and structure of TML sequence homologs (A) Analysis by the maximum likelihood method using sequence homologs from public databases (Supplemental Table 1) as described in Methods, in *M. truncatula* (Mt), *Arabidopsis thaliana* (At), *Nicotiana tobacum* (Nt), *Pisum sativum* (Ps), *Trifolium pratense* (Tp), *Glycine max* (Gm), *Phaseolus vulgaris* (Pv), *Solanum lycopersicum* (Sl), *Populus trichocarpa* (Pt), *Zea mays* (Zm), *Oryza sativa* (Os), and *Sorghum bicolor* (Sb). Percentage of replicate trees in which the associated taxa clustered together in the bootstrap test 1000 replicates are shown next to the branches. B) Structural prediction of TML1 protein best ranked models as determined by AlphaFold. The range of predicted local distance difference test (pLDDT) scores are 83.3 – 84.7. C) Structural prediction of TML 2 protein best ranked models as determined by AlphaFold. The range of predicted local distance difference test (pLDDT) scores are 81.0 – 82.2. D) AlphaFold Multimer highest ranked interaction of TML1 and TML2. The range of values for the per-structure quality estimate score or interface predicted template modeling score (ipTM) were 0.238 – 0.395 which is below the stringency cutoff value. Arrows in B and C indicate the kelch repeats, better visualized in movies which allow rotation of the structure in Supplemental Figure 1.

Figure 2. *TML* alleles used in this work. Diagrams are based on the translation of the R108 genotype sequence of Medtr7g029290 (*MtTML1*) and Medtr6g023805 (*MtTML2*). Protein features

are shown by colored boxes: F-box in orange, kelch repeats in blue, Nuclear Localization signal (NLS) in green. miRNA2111 binding sites are in the coding sequence (CDS) indicated in Supplemental Figure 2. (A) *TML1* alleles. *tml1-1* is a 14 bp deletion combined with a 2 bp deletion resulting in an amino acid change and stop at aa13. *tml1-2* is a 334 bp deletion with the addition of an A that results in a V to K change at amino acid 11, and deletion of 111 amino acids, removing the F-box and NLS. *tml1-3* is a 1 bp deletion that also creates a stop at the same codon as *tml1-1*. *tml1-4* is a 104 bp deletion in the 5' UTR and beginning of the coding sequence that removes the start codon and the first 20 amino acids. (B) *tml2-1* is a *Tnt1* insertion 119 bp from the start of the coding region resulting in addition of 20 new amino acids starting at position 47 before eventually terminating the protein at position 67. *tml2-2* is an insertion of a C, creating a stop codon at amino acid position 60 in the F box, likewise *tml2-3* is a 1bp deletion that creates a stop at amino acid 61 in the F box. Creation of the CRISPR alleles is detailed in Supplemental Figure 1. (C) Double mutant combinations used in the analysis.

Figure 3. Phenotype of single and double mutant alleles in *MtTML1* and *MtTML2* genes. (A) whole plants displaying root nodules at 10dpi in an aeroponic system inoculated with *Sinorhizobium meliloti* strain RM41. Two representative plants per genotype L to R: R108 (wild type), *tml1-2*, *tml1-3*, *tml1-4*, *tml2-1*, *tml2-2*, *tml1-1 tml2-3*, *tml1-1 tml2-2*, *tml1-2 tml2-2* and *sunn-5.* Scale bar = 2 cm. (B-H) magnification of nodules from a representative plant for genotypes (B) R108, (C) *tml1-2*, (D) *tml1-4*, (E) *tml2-1*, (F) *tml2-2*, (G) *tml1-1 tml2-3*, and (H) *tml1-2 tml2-2*. A single root was folded in (G) and (H) to show wider area of nodulation in same picture.; B to H scale bar = 2mm.

Figure 4. Nodulation and root length phenotypes of single and double mutant lines in *MtTML1* and *MtTML2* genes under different conditions. (A) Nodule number and (B) root

length at 10dpi of wild type, single mutant, and double mutant plants from the same experiment in Figure 3. N = 6 – 9 plants for *tml1-2*, *tml1-1 tml2-2*, and *tml1-1 tml2-3*; N = 10-19 plants for remaining genotypes. (C) Nodulation phenotype presence of 10 mM N (5mM NH_4NO_3) at 10dpi. N = 5 to 10 plants per genotype (D) Comparison of A and C-nodulation with sufficient N (10 mM) as a percent of nodulation under normal conditions (0 mM N). (E) Root length (in mm) at the same developmental time but no rhizobial inoculation and sufficient N (10 mM). Dots indicate values for individual plants. N = 18 to 22 plants per genotype. Significant difference between means were tested by Student's t-test followed by Bonferroni correction of multiple t-test (**$p<0.01$, ***$p<0.001$). Dots indicate values for individual plants, A and C contain insert enlargement to show y-axis detail.

Figure 5. Spatiotemporal and differential expression of *MtTML* genes over 72 hours in plants responding to rhizobia (A) Diagrams produced from ePlant resource (Schnabel et al., 2023) with gradient display adjusted to identical color representation to allow comparison of the expression levels as well as localization of *TML1* and *TML2* across time in wild type roots responding to rhizobia up to 72 hpi. (B) Transcriptomics data re-graphed from (Schnabel et al., 2023) showing *TML* expression in whole root segments under the same conditions. The average FPKMs of three libraries are shown for five time points for uninoculated and inoculated (wild type A17 and *sunn-4*) root segments. Both genes had $p < 0.05$ (DeSeq2) for at least one time point between uninoculated and inoculated samples. (C) Heat Map of relative abundance of single cells expressing *TML* genes by cell type cluster. The heat map is generated from single cell RNASeq data collected from *M. truncatula* roots undergoing nodulation over 96 hours in a similar system, using a function created in shinyapp and reported in (Pereira et al., 2023). Cell cluster number tissue type identification and is as reported in (Pereira et al., 2023). VSC=very small cluster. (D)

Relative expression of *TML1* in a *tml2-2* mutant at 0 and 72 hours post inoculation (hpi), normalized to wild type at 0 hpi. (E) Relative expression of *TML2* in a *tml1-4* mutant at 0 and 72 hours post inoculation normalized to wild type at 0 hpi. Note difference in scale between A and B. ** $p < 0.05$. Each graph is the results from 3 technical replicates each of 3 biological replicates compared to the reference gene PIK.

Figure 6. Distribution of nodulation number phenotypes demonstrates heterozygous effect. (A) Distribution plots of two populations of progeny from selfing of plant on X axis. Red dots are individual plant nodules numbers from *tml2-2* mutant plants segregating one wild type *TML1* allele, blue squares are *tml1-2* mutants segregating one wild type *TML2* allele. (B) *TML1* segregating population from A (red dots in both plots) broken down by molecular genotype. Blue are homozygous wild type *TML1,* green are heterozygous *tml1/TML1* and black are homozygous *tml1/tml1*. Lines indicate median nodule number for each group. A representative photo of plant phenotypes appears in Supplemental Figure 3.

Figure 7. Arbuscular mycorrhiza symbiosis is not impaired in *tml1-1, tml2-2* double mutants. A) Overall root length colonization is similar in *tml1-1; tml2-2* double mutants and R108 wild-types. Student's t-test $p>0.05$ (not significant, n.s.). B) Arbuscule density (defined as arbuscules per mm of colonized root length) is not changed in *tml1-1; tml2-2* double mutants relative to R108 wild-type. Student's t-test $p>0.05$ (not significant, n.s.). C) Representative image of *Rhizophagus irregularis* symbiotic structures in an R108 wild-type root. D) Representative image of a *R. irregularis*-colonized root of a *tml1-1 tml2-2* double mutant. C, D) *R. irregularis* fungal structures

are visualized with WGA-Alexafluor488. *M. truncatula* root is outlined with a dashed line. Scale bar: 100µm.

Figure 8. Model for Autoregulation Signaling in symbiosis. Both rhizobial symbiosis (blue) and arbuscular mycorrhizal symbiosis (green) auto- and nutrient-regulation signal through the SUNN receptor kinase, but the presumed CLE peptide ligands for SUNN are different, and the data suggest that autoregulation downstream of SUNN bifurcates. See discussion for details.

Supplemental Materials:

Supplemental Figure 1. Rotational movie views of protein models. (A) TML1 (B) TML2 (C) TML1:TML2 dimer. The same structures are presented in Figure 1. These views allow rotational examination of AlphaFold best ranked predicted structures.

Supplemental Figure 2. Multiplexed targeted CRISPR/Cas9 mutagenesis in *TML* genes using Csy4. (A) Schematic diagram of polycistronic gene construct used in pDIRECT_23C+TML1/2 for making *tml1/tml2* double mutants and (B) in pDIRECT_23C+TML1 for making *tml1* mutant (C) Maps of *MtTML1* and *MtTML2* genes showing the location of targets. PAM for each target is underlined. Blue boxes indicate CDS, grey boxes indicate UTR, red rectangles indicate predicted miRNA2111 binding sites, and lines indicate introns; arrow at the right end of grey box points to 3' end of gene. (D) CRISPR effects on DNA resulting in *tml1* alleles, displayed in relation to the target sequences (yellow) and PAM sequences (green). Base changes and deletions are in red. The *tml1-4* allele has a 107 bp deletion that removes 48bp upstream of the transcription start site and 59bp in the CDS, including target 1. (E) CRISPR effects on DNA resulting in *tml2* alleles, displayed in relation to the target sequences (yellow) and PAM sequences (green). Base changes and deletions are in red.

Supplemental Figure 3. Phenotype of single, double and heterozygous in one gene but homozygous in other *TML* gene. Whole plants displaying root nodules at 10dpi in an aeroponic system inoculated with *Sinorhizobium meliloti* strain RM41. (A) One representative plant per genotype L to R: R108 (wild type), *tml1-2*, tml1-2 tml2-2 het, tml1-2 tml2-2 and (B) R108 (wild type), *tml2-2*, tml1-2 het *tml2-2*, and *tml1-2 tml2-2*. Scale bar = 2 cm.

Supplemental Table 1. Genes used in Maximum Likelihood tree in Figure 1

Supplemental Table 2. Primers used in this manuscript

References

Bashyal S, Gautam CK, Müller LM (2023) CLAVATA signaling in plant–environment interactions. Plant Physiology**:** kiad591

Cai J, Veerappan V, Arildsen K, Sullivan C, Piechowicz M, Frugoli J, Dickstein R (2023) A Modified Aeroponic System for Growing Plants to Study Root Systems. Plant Methods

Catford J-G, Staehelin C, Lerat S, Piché Y, Vierheilig H (2003) Suppression of arbuscular mycorrhizal colonization and nodulation in split-root systems of alfalfa after pre-innoculation and treatment with Nod factors. Journal of Experimental Botany **54:** 1481-1487

Chaulagain D, Frugoli J (2021) The Regulation of Nodule Number in Legumes Is a Balance of Three Signal Transduction Pathways. International Journal of Molecular Sciences

Chaulagain D, Schnabel E, Crook A, Bashyal S, Müller L, Frugoli J (2023) A Mutation in Mediator Subunit MED16A Suppresses Nodulation and Increases Arbuscule Density in Medicago truncatula. Journal of Plant Growth Regulation**:** 1-19

Crook AD, Schnabel EL, Frugoli JA (2016) The systemic nodule number regulation kinase SUNN in Medicago truncatula interacts with MtCLV2 and MtCRN. Plant Journal **88:** 108-119

El-Brolosy MA, Kontarakis Z, Rossi A, Kuenne C, Günther S, Fukuda N, Kikhi K, Boezio GL, Takacs CM, Lai S-L (2019) Genetic compensation triggered by mutant mRNA degradation. Nature **568:** 193-197

Engler C, Gruetzner R, Kandzia R, Marillonnet S (2009) Golden gate shuffling: a one-pot DNA shuffling method based on type IIs restriction enzymes. PloS One **4:e5553**

Engler C, Kandzia R, Marillonnet S (2008) A one pot, one step, precision cloning method with high throughput capability. PloS One **3: e3647**

Evans R, O'Neill M, Pritzel A, Antropova N, Senior A, Green T, Žídek A, Bates R, Blackwell S, Yim J, Ronneberger O, Bodenstein S, Zielinski M, Bridgland A, Potapenko A, Cowie A, Tunyasuvunakool K, Jain R, Clancy E, Kohli P, Jumper J,

Hassabis D (2022) Protein complex prediction with AlphaFold-Multimer. bioRxiv**:** 2021.2010.2004.463034

Ferguson BJ, Mens C, Hastwell AH, Zhang M, Su H, Jones CH, Chu X, Gresshoff PM (2019) Legume nodulation: the host controls the party. Plant, cell & environment **42:** 41-51

Gautrat P, Laffont C, Frugier F (2020) Compact Root Architecture 2 Promotes Root Competence for Nodulation through the miR2111 Systemic Effector. Current Biology **30:** 1339-1345.e1333

Gautrat P, Laffont C, Frugier F, Ruffel S (2021) Nitrogen Systemic Signaling: From Symbiotic Nodulation to Root Acquisition. Trends in Plant Science **26:** 392-406

Gautrat P, Mortier V, Laffont C, De Keyser A, Fromentin J, Frugier F, Goormachtig S (2019) Unraveling new molecular players involved in the autoregulation of nodulation in Medicago truncatula. Journal of Experimental Botany **70:** 1407-1417

Hood EE, Gelvin SB, Melchers LS, Hoekema A (1993) New Agrobacterium Helper Plasmids for Gene-Transfer to Plants. Transgenic Research **2:** 208-218

Hsieh L-C, Lin S-I, Shih AC-C, Chen J-W, Lin W-Y, Tseng C-Y, Li W-H, Chiou T-J (2009) Uncovering small RNA-mediated responses to phosphate deficiency in Arabidopsis by deep sequencing. Plant physiology **151:** 2120-2132

Ivanovici A, Laffont C, Larrainzar E, Patel N, Winning CS, Lee H-C, Imin N, Frugier F, Djordjevic MA (2023) The Medicago SymCEP7 hormone increases nodule number via shoots without compromising lateral root number. Plant Physiology **191:** 2012-2026

Ivanovici ASL (2021) Signals and perCEPtion: diverse roles for C-Terminally Encoded Peptides in symbiosis, root system gravitropism, and pathogen response in Medicago truncatula and Arabidopsis thaliana. The Australian National University (Australia)

Jumper J, Evans R, Pritzel A, Green T, Figurnov M, Ronneberger O, Tunyasuvunakool K, Bates R, Žídek A, Potapenko A (2021) Highly accurate protein structure prediction with AlphaFold. Nature **596:** 583-589

Kakar K, Wandrey M, Czechowski T, Gaertner T, Scheible W-R, Stitt M, Torres-Jerez I, Xiao Y, Redman JC, Wu HC, Cheung F, Town CD, Udvardi MK (2008) A community resource for high-throughput quantitative RT-PCR analysis of transcription factor gene expression in Medicago truncatula. Plant Methods **4:** 18

Karlo M, Boschiero C, Landerslev KG, Blanco GS, Wen J, Mysore KS, Dai X, Zhao PX, de Bang TC (2020) The CLE53–SUNN genetic pathway negatively regulates arbuscular mycorrhiza root colonization in Medicago truncatula. Journal of Experimental Botany **71:** 4972-4984

Kassaw T, Bridges W, Frugoli J (2015) Multiple autoregulation of nodulation (AON) signals identified through split root analysis of M. truncatula sunn and rdn1 mutants. Plants **4:** 209-224

Kassaw T, Nowak S, Schnabel E, Frugoli J (2017) ROOT DETERMINED NODULATION1 Is Required for M. truncatula CLE12, But Not CLE13, Peptide Signaling through the SUNN Receptor Kinase. Plant Physiol **174:** 2445-2456

Laffont C, Frugier F (2023) Rhizobium symbiotic efficiency meets CEP signaling peptides. New Phytologist

Laffont C, Huault E, Gautrat P, Endre G, Kalo P, Bourion V, Duc G, Frugier F (2019) Independent Regulation of Symbiotic Nodulation by the SUNN Negative and CRA2 Positive Systemic Pathways. Plant Physiology **180:** 559-570

Laffont C, Ivanovici A, Gautrat P, Brault M, Djordjevic MA, Frugier F (2020) The NIN transcription factor coordinates CEP and CLE signaling peptides that regulate nodulation antagonistically. Nature Communications **11**

Lepetit M, Brouquisse R (2023) Control of the rhizobium–legume symbiosis by the plant nitrogen demand is tightly integrated at the whole plant level and requires inter-organ systemic signaling. Frontiers in Plant Science **14**

Lin J-s, Li X, Luo Z, Mysore KS, Wen J, Xie F (2018) NIN interacts with NLPs to mediate nitrate inhibition of nodulation in Medicago truncatula. Nature plants **4:** 942-952

Ma X, Liu YG (2016) CRISPR/Cas9-based multiplex genome editing in monocot and dicot plants. Current protocols in molecular biology **115:** 31.36. 31-31.36. 21

Magori S, Oka-Kira E, Shibata S, Umehara Y, Kouchi H, Hase Y, Tanaka A, Sato S, Tabata S, Kawaguchi M (2009) TOO MUCH LOVE, a root regulator associated with the long-distance control of nodulation in Lotus japonicus. Molecular Plant-Microbe Interactions **22:** 259-268

McGonigle TP, Miller MH, Evans DG, Fairchild GL, Swan JA (1990) A new method which gives an objective measure of colonization of roots by vesicular—arbuscular mycorrhizal fungi. New Phytologist **115:** 495-501

Meixner C, Ludwig-Müller J, Miersch O, Gresshoff P, Staehelin C, Vierheilig H (2005) Lack of mycorrhizal autoregulation and phytohormonal changes in the supernodulating soybean mutant nts1007. Planta **222:** 709-715

Morandi D, Sagan M, Prado-Vivant E, Duc G (2000) Influence of genes determining supernodulation on root colonization by the mycorrhizal fungus Glomus mosseae in Pisum sativum and Medicago truncatula mutants. Mycorrhiza **10:** 37-42

Moreau C, Gautrat P, Frugier F (2021) Nitrate-induced CLE35 signaling peptides inhibit nodulation through the SUNN receptor and miR2111 repression. Plant Physiology **185:** 1216-1228

Mortier V, De Wever E, Vuylsteke M, Holsters M, Goormachtig S (2012) Nodule numbers are governed by interaction between CLE peptides and cytokinin signaling. Plant J **70:** 367-376

Mortier V, Den Herder G, Whitford R, Van de Velde W, Rombauts S, D'Haeseleer K, Holsters M, Goormachtig S (2010) CLE peptides control Medicago truncatula nodulation locally and systemically. Plant Physiol **153:** 222-237

Müller LM, Flokova K, Schnabel E, Sun X, Fei Z, Frugoli J, Bouwmeester HJ, Harrison MJ (2019) A CLE–SUNN module regulates strigolactone content and fungal colonization in arbuscular mycorrhiza. Nature Plants **5:** 933-939

Nishida H, Ito M, Miura K, Kawaguchi M, Suzaki T (2020) Autoregulation of nodulation pathway is dispensable for nitrate-induced control of rhizobial infection. Plant signaling & behavior **15:** 1733814

Nishida H, Tanaka S, Handa Y, Ito M, Sakamoto Y, Matsunaga S, Betsuyaku S, Miura K, Soyano T, Kawaguchi M, Suzaki T (2018) A NIN-LIKE PROTEIN mediates nitrate-induced control of root nodule symbiosis in Lotus japonicus. Nature Communications **9:** 499

Nowak S, Schnabel E, Frugoli J (2019) The Medicago truncatula CLAVATA3-LIKE CLE12/13 signaling peptides regulate nodule number depending on the CORYNE but not the COMPACT ROOT ARCHITECTURE2 receptor. Plant signaling & behavior **14:** 1598730

O'Reilly FJ, Graziadei A, Forbrig C, Bremenkamp R, Charles K, Lenz S, Elfmann C, Fischer L, Stülke J, Rappsilber J (2023) Protein complexes in cells by AI-assisted structural proteomics. Molecular Systems Biology **19:** e11544

Okuma N, Kawaguchi M (2021) Systemic optimization of legume nodulation: A shoot-derived regulator, miR2111. Frontiers in Plant Science **12:** 682486

Okuma N, Soyano T, Suzaki T, Kawaguchi M (2020) MIR2111-5 locus and shoot-accumulated mature miR2111 systemically enhance nodulation depending on HAR1 in Lotus japonicus. Nature Communications **11:** 5192

Oldroyd GE, Leyser O (2020) A plant's diet, surviving in a variable nutrient environment. Science **368:** eaba0196

Pant BD, Musialak-Lange M, Nuc P, May P, Buhtz A, Kehr J, Walther D, Scheible W-Rd (2009) Identification of nutrient-responsive Arabidopsis and rapeseed microRNAs by comprehensive real-time polymerase chain reaction profiling and small RNA sequencing. Plant physiology **150:** 1541-1555

Pereira WJ, Boyd J, Conde D, Triozzi PM, Balmant KM, Dervinis C, Schmidt HW, Boaventura-Novaes C, Chakraborty S, Knaack SA (2023) The Single-Cell Transcriptome Program of Nodule Development Cellular Lineages in Medicago truncatula. bioRxiv**:** 2023.2006. 2013.544787

Putnoky P, Petrovics G, Kereszt A, Grosskopf E, Ha D, Banfalvi Z, Kondorosi A (1990) Rhizobium meliloti lipopolysaccharide and exopolysaccharide can have the same function in the plant-bacterium interaction. Journal of bacteriology **172:** 5450-5458

Pérez-Pérez JM, Candela H, Micol JL (2009) Understanding synergy in genetic interactions. Trends in genetics **25:** 368-376

Roy S, Liu W, Nandety RS, Crook A, Mysore KS, Pislariu CI, Frugoli J, Dickstein R, Udvardi MK (2020) Celebrating 20 years of genetic discoveries in legume nodulation and symbiotic nitrogen fixation. The Plant Cell **32:** 15-41

Roy S, Müller LM (2022) A rulebook for peptide control of legume–microbe endosymbioses. Trends in plant science

Schnabel E, Journet EP, Carvalho-Niebel F, Duc G, Frugoli J (2005) The Medicago truncatula SUNN gene encoding a CLV1-like leucine-rich repeat receptor kinase regulates both nodule number and root length. Plant Molecular Biology **58:** 809-822

Schnabel E, Kassaw T, Smith L, Marsh J, Oldroyd G, Long S, Frugoli J (2011) The ROOT DETERMINED NODULATION 1 gene regulates nodule number in roots of Medicago truncatula and defines a highly conserved, uncharacterized plant gene family. Plant Physiology **157:** 328-340

Schnabel E, Mukherjee A, Smith L, Kassaw T, Long S, Frugoli J (2010) The lss supernodulation mutant of Medicago truncatula reduces expression of the SUNN gene. Plant Physiol **154:** 1390-1402

Schnabel E, Thomas J, El-Hawaz R, Gao Y, Poehlman W, Chavan S, Pasha A, Esteban E, Provart NL, Feltus FA (2023) Laser capture microdissection transcriptome reveals spatiotemporal tissue gene expression patterns of M. truncatula roots responding to rhizobia. Molecular Plant-Microbe Interactions

Schnabel EL, Chavan SA, Gao Y, Poehlman WL, Feltus FA, Frugoli JA (2023) A Medicago truncatula Autoregulation of Nodulation Mutant Transcriptome Analysis Reveals Disruption of the SUNN Pathway Causes Constitutive Expression Changes in Some

Genes, but Overall Response to Rhizobia Resembles Wild-Type, Including Induction of TML1 and TML2. Current Issues in Molecular Biology **45:** 4612-4631

Shultz JL, Kurunam D, Shopinski K, Iqbal MJ, Kazi S, Zobrist K, Bashir R, Yaegashi S, Lavu N, Afzal AJ (2006) The Soybean Genome Database (SoyGD): a browser for display of duplicated, polyploid, regions and sequence tagged sites on the integrated physical and genetic maps of Glycine max. Nucleic Acids Research **34:** D758-D765

Tadege M, Wen JQ, He J, Tu HD, Kwak Y, Eschstruth A, Cayrel A, Endre G, Zhao PX, Chabaud M, Ratet P, Mysore KS (2008) Large-scale insertional mutagenesis using the Tnt1 retrotransposon in the model legume Medicago truncatula. Plant Journal **54:** 335-347

Takahara M, Magori S, Soyano T, Okamoto S, Yoshida C, Yano K, Sato S, Tabata S, Yamaguchi K, Shigenobu S, Takeda N, Suzaki T, Kawaguchi M (2013) Too much love, a novel Kelch repeat-containing F-box protein, functions in the long-distance regulation of the legume-Rhizobium symbiosis. Plant Cell Physiol **54:** 433-447

Tamura K, Stecher G, Kumar S (2021) MEGA11: Molecular Evolutionary Genetics Analysis Version 11. Molecular Biology and Evolution **38:** 3022-3027

Tang H, Krishnakumar V, Bidwell S, Rosen B, Chan A, Zhou S, Gentzbittel L, Childs KL, Yandell M, Gundlach H (2014) An improved genome release (version Mt4. 0) for the model legume Medicago truncatula. BMC genomics **15:** 1-14

Tiwari M, Pandey V, Singh B, Bhatia S (2021) Dynamics of miRNA mediated regulation of legume symbiosis. Plant, Cell & Environment **44:** 1279-1291

Tsikou D, Yan Z, Holt DB, Abel NB, Reid DE, Madsen LH, Bhasin H, Sexauer M, Stougaard J, Markmann K (2018) Systemic control of legume susceptibility to rhizobial infection by a mobile microRNA. Science **362:** 233-236

Varadi M, Anyango S, Deshpande M, Nair S, Natassia C, Yordanova G, Yuan D, Stroe O, Wood G, Laydon A (2022) AlphaFold Protein Structure Database: massively expanding the structural coverage of protein-sequence space with high-accuracy models. Nucleic acids research **50:** D439-D444

Wang C, Reid JB, Foo E (2018) The Art of Self-Control – Autoregulation of Plant–Microbe Symbioses. Frontiers in Plant Science **9:** 988

Wang C, Velandia K, Kwon C-T, Wulf KE, Nichols DS, Reid JB, Foo E (2021) The role of CLAVATA signalling in the negative regulation of mycorrhizal colonization and nitrogen response of tomato. Journal of Experimental Botany **72:** 1702-1713

Wen L, Chen Y, Schnabel E, Crook AD, Frugoli J (2019) Comparison of efficiency and time to regeneration of Agrobacterium-mediated transformation methods in Medicago truncatula. Plant Methods **15**

Wolfe KH, Gouy M, Yang Y-W, Sharp PM, Li W-H (1989) Date of the monocot-dicot divergence estimated from chloroplast DNA sequence data. Proceedings of the National Academy of Sciences **86:** 6201-6205

Yan D, Nambara E (2023) Conserved and unique functions of NIN-like proteins in nitrate sensing and signaling. Plant Science**:** 111842

Zakaria Solaiman M, Senoo K, Kawaguchi M, Imaizumi-Anraku H, Akao S, Tanaka A, Obata H (2000) Characterization of mycorrhizas formed by Glomus sp. on roots of hypernodulating mutants of Lotus japonicus. Journal of plant research **113:** 443-448

Zhu W, Shenoy A, Kundrotas P, Elofsson A (2023) Evaluation of AlphaFold-Multimer prediction on multi-chain protein complexes. Bioinformatics **39**

Čermák T, Curtin SJ, Gil-Humanes J, Čegan R, Kono TJ, Konečná E, Belanto JJ, Starker CG, Mathre JW, Greenstein RL (2017) A multipurpose toolkit to enable advanced genome engineering in plants. The Plant Cell **29:** 1196-1217

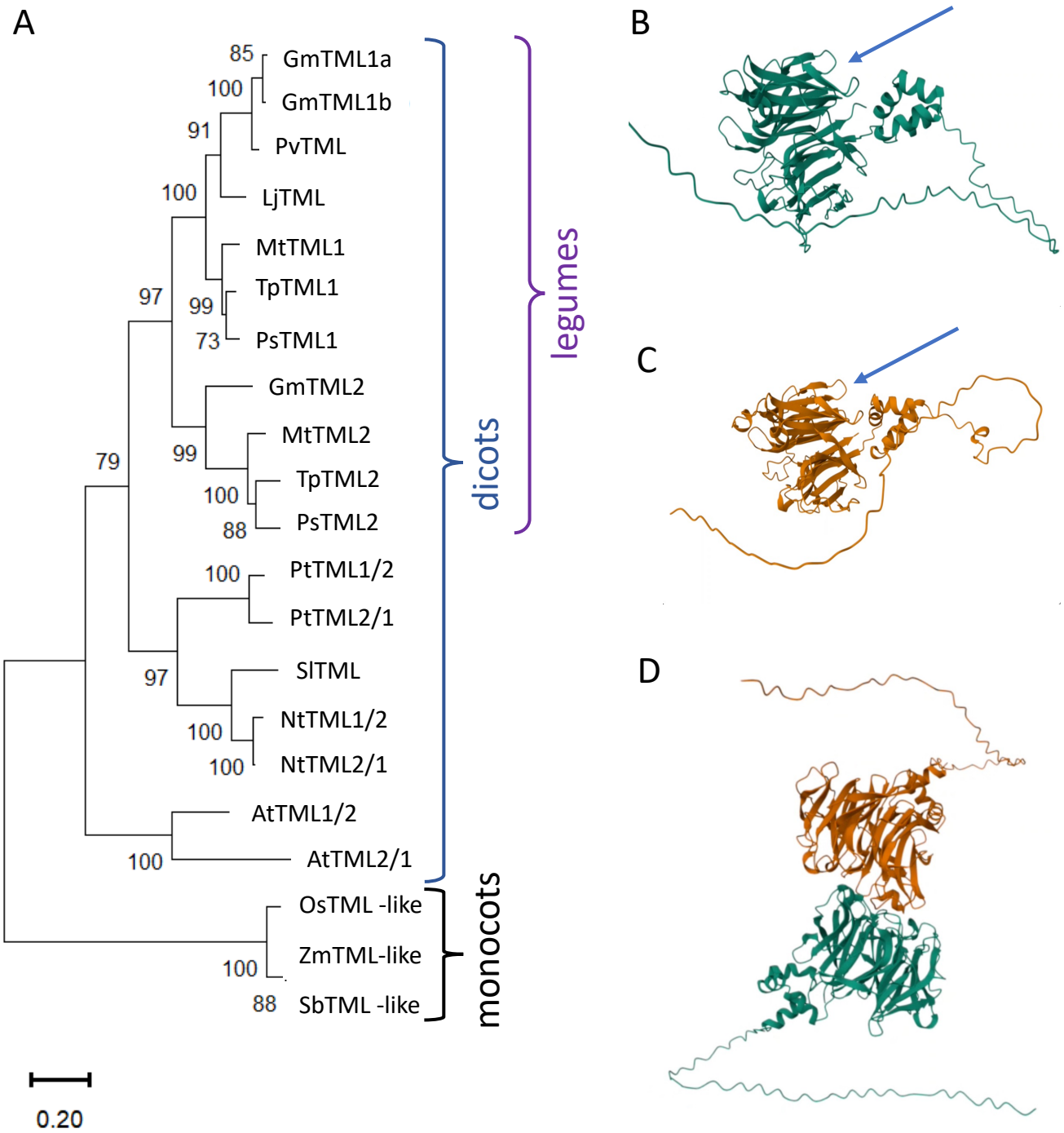

Figure 1: Phylogenetic analysis and structure of TML sequence homologs (A) Analysis by the maximum likelihood method using sequence homologs from public databases (Supplemental Table 1) as described in Methods, in *M. truncatula* (Mt), *Arabidopsis thaliana* (At), *Nicotiana tobacum* (Nt), *Pisum sativum* (Ps), *Trifolium pratense* (Tp), *Glycine max* (Gm), *Phaseolus vulgaris* (Pv), *Solanum lycopersicum* (Sl), *Populus trichocarpa* (Pt), *Zea mays* (Zm), *Oryza sativa* (Os), and *Sorghum bicolor* (Sb). Percentage of replicate trees in which the associated taxa clustered together in the bootstrap test 1000 replicates are shown next to the branches. B) Structural prediction of TML1 protein best ranked models as determined by AlphaFold. The range of predicted local distance difference test (pLDDT) scores are 83.3 – 84.7. C) Structural prediction of TML 2 protein best ranked models as determined by AlphaFold. The range of predicted local distance difference test (pLDDT) scores are 81.0 – 82.2. D) AlphaFold Multimer highest ranked interaction of TML1 and TML2. The range of values for the per-structure quality estimate score or interface predicted template modeling score (ipTM) were 0.238 – 0.395 which is below the stringency cutoff value. Arrows in B and C indicate the kelch repeats, better visualized in movies which allow rotation of the structure in Supplemental Figure 1.

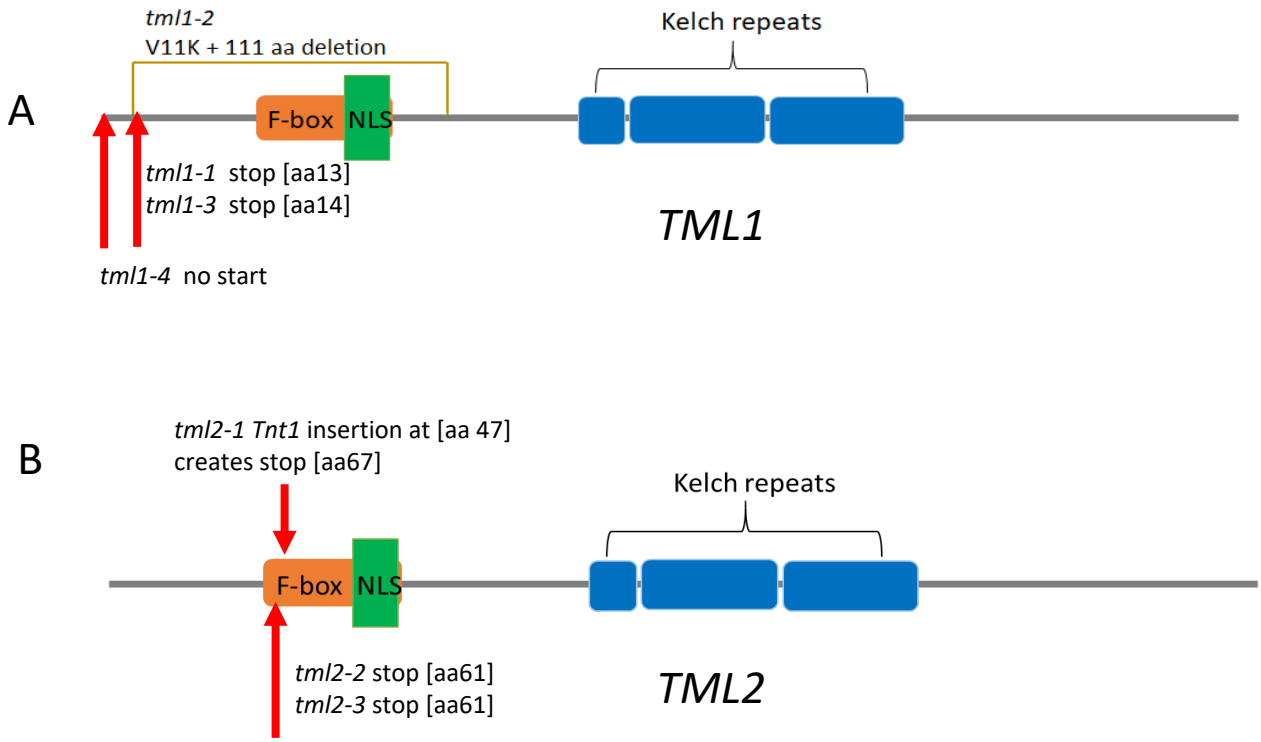

C

Double mutants	protein
tml1-1 tml2-2	Both early stops
tml1-2 tml 2-2	Large deletion & stop
tml1-1 tml2-3	Both early stops

Figure 2. *TML* alleles used in this work. Diagrams are based on the translation of the R108 genotype sequence of Medtr7g029290 (*MtTML1*) and Medtr6g023805 (*MtTML2*). Protein features are shown by colored boxes: F-box in orange, kelch repeats in blue, Nuclear Localization signal (NLS) in green. miRNA2111 binding sites are in the coding sequence (CDS) indicated in Supplemental Figure 2. (A) *TML1* alleles. *tml1-1* is a 14 bp deletion combined with a 2 bp deletion resulting in an amino acid change and stop at aa13. *tml1-2* is a 334 bp deletion with the addition of an A that results in a V to K change at amino acid 11, and deletion of 111 amino acids, removing the F-box and NLS. *tml1-3* is a 1 bp deletion that also creates a stop at the same codon as *tml1-1*. *tml1-4* is a 104 bp deletion in the 5' UTR and beginning of the coding sequence that removes the start codon and the first 20 amino acids. (B) *tml2-1* is a *Tnt1* insertion 119 bp from the start of the coding region resulting in addition of 20 new amino acids starting at position 47 before eventually terminating the protein at position 67. *tml2-2* is an insertion of a C, creating a stop codon at amino acid position 60 in the F box, likewise *tml2-3* is a 1bp deletion that creates a stop at amino acid 61 in the F box. Creation of the CRISPR alleles is detailed in Supplemental Figure 1. (C) Double mutant combinations used in the analysis.

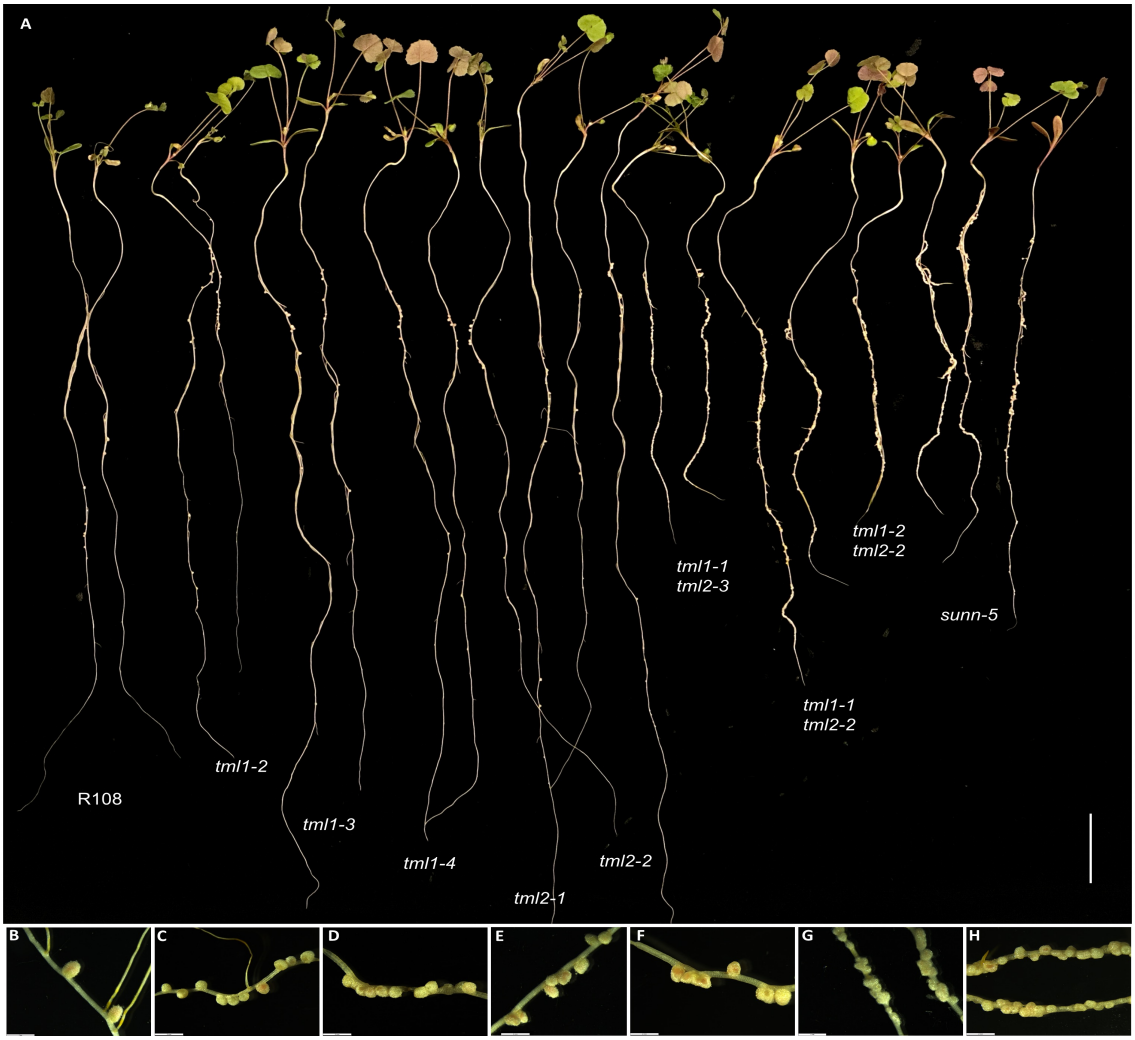

Figure 3. Phenotype of single and double mutant alleles in *MtTML1* and *MtTML2* genes. (A) whole plants displaying root nodules at 10dpi in an aeroponic system inoculated with *Sinorhizobium meliloti* strain RM41. Two representative plants per genotype L to R: R108 (wild type), *tml1-2*, *tml1-3*, *tml1-4*, *tml2-1*, *tml2-2*, *tml1-1 tml2-3*, *tml1-1 tml2-2*, *tml1-2 tml2-2* and *sunn-5.* Scale bar = 2 cm. (B-H) magnification of nodules from a representative plant for genotypes (B) R108, (C) *tml1-2*, (D) *tml1-4*, (E) *tml2-1*, (F) *tml2-2*, (G) *tml1-1 tml2-3*, and (H) *tml1-2 tml2-2*. A single root was folded in (G) and (H) to show wider area of nodulation in same picture.; B to H scale bar = 2mm.

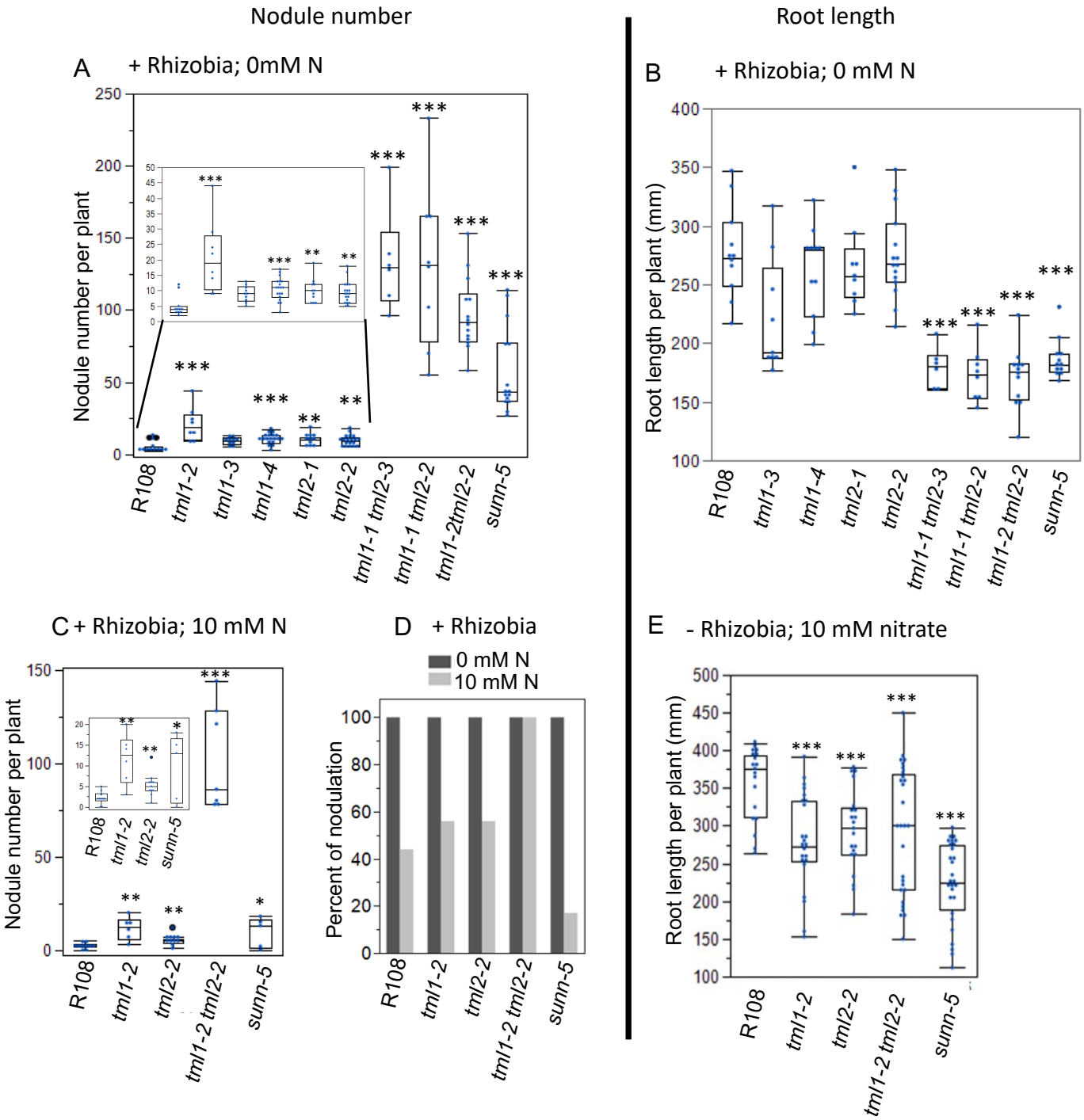

Figure 4. Nodulation and root length phenotypes of single and double mutant lines in *MtTML1* and *MtTML2* genes under different conditions. (A) Nodule number and (B) root length at 10dpi of wild type, single mutant, and double mutant plants from the same experiment in Figure 3. N = 6 – 9 plants for *tml1-2*, *tml1-1 tml2-2*, and *tml1-1 tml2-3*; N = 10-19 plants for remaining genotypes. (C) Nodulation phenotype presence of 10 mM N (5mM NH_4NO_3) at 10dpi. N = 5 to 10 plants per genotype (D) Comparison of A and C-nodulation with sufficient N (10 mM) as a percent of nodulation under normal conditions (0 mM N). (E) Root length (in mm) at the same developmental time but no rhizobial inoculation and sufficient N (10 mM). Dots indicate values for individual plants. N = 18 to 22 plants per genotype. Significant difference between means were tested by Student's t-test followed by Bonferroni correction of multiple t-test (*p<0.05, **p<0.01, ***p<0.001). Dots indicate values for individual plants, A and C contain insert enlargement to show y-axis detail.

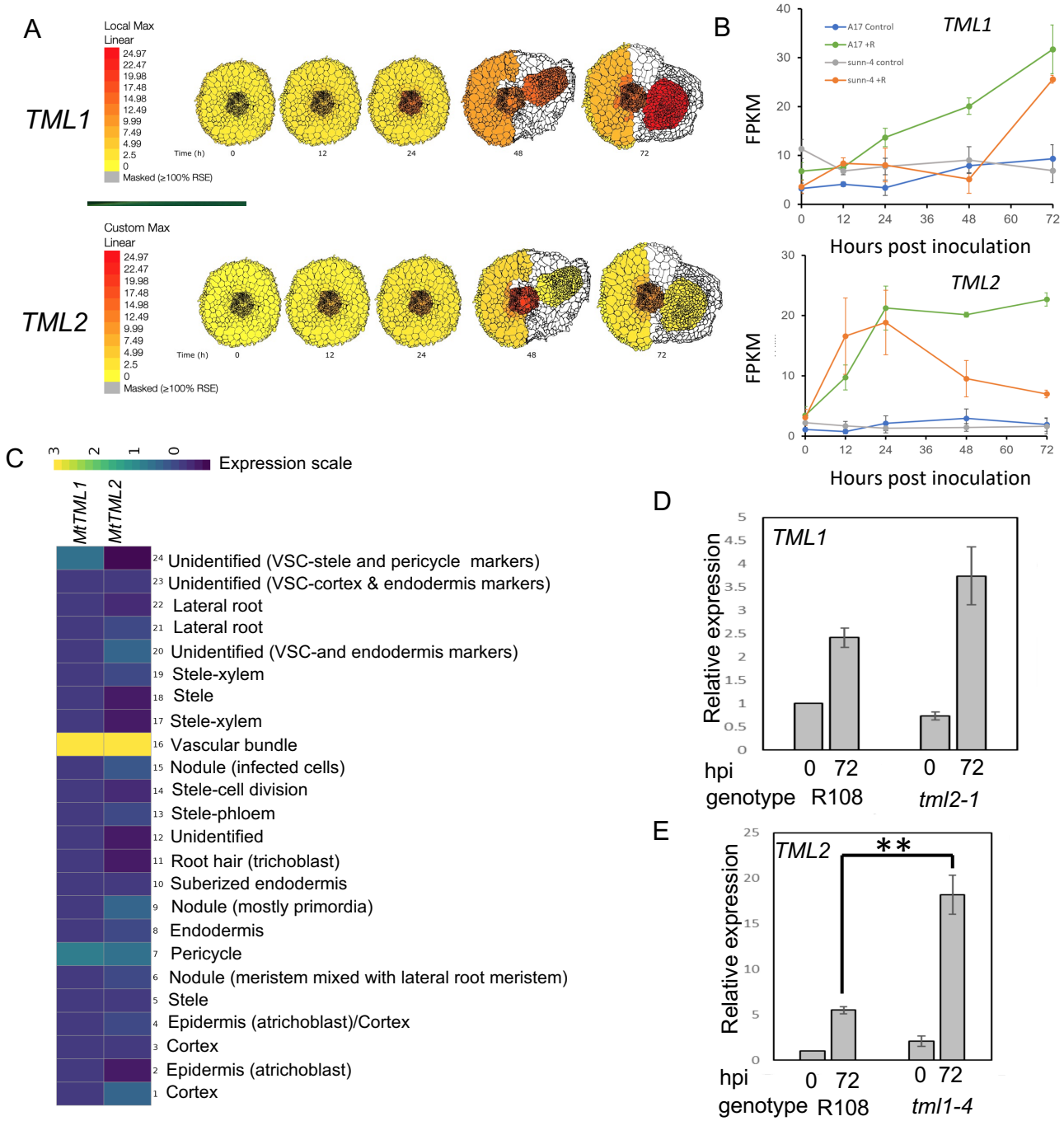

Figure 5. Spatiotemporal and differential expression of *MtTML* genes over 72 hours in plants responding to rhizobia (A) Diagrams produced from ePlant resource (Schnabel et al., 2023) with gradient display adjusted to identical color representation to allow comparison of the expression levels as well as localization of *TML1* and *TML2* across time in wild type roots responding to rhizobia up to 72 hpi. (B) Transcriptomics data re-graphed from (Schnabel et al., 2023) showing *TML* expression in whole root segments under the same conditions. The average FPKMs of three libraries are shown for five time points for uninoculated and inoculated (wild type A17 and *sunn-4*) root segments. Both genes had $p < 0.05$ (DeSeq2) for at least one time point between uninoculated and inoculated samples. (C) Heat Map of relative abundance of single cells expressing *TML* genes by cell type cluster. The heat map is generated from single cell RNASeq data collected from *M. truncatula* roots undergoing nodulation over 96 hours in a similar system, using a function created in shinyapp and reported in (Pereira et al., 2023). Cell cluster number tissue type identification and is as reported in (Pereira et al., 2023). VSC=very small cluster. (D) Relative expression of *TML1* in a *tml2-2* mutant at 0 and 72 hours post inoculation (hpi), normalized to wild type at 0 hpi. (E) Relative expression of *TML2* in a *tml1-4* mutant at 0 and 72 hours post inoculation normalized to wild type at 0 hpi. Note difference in scale between A and B. ** $p < 0.05$. Each graph is the results from 3 technical replicates each of 3 biological replicates compared to the reference gene PIK.

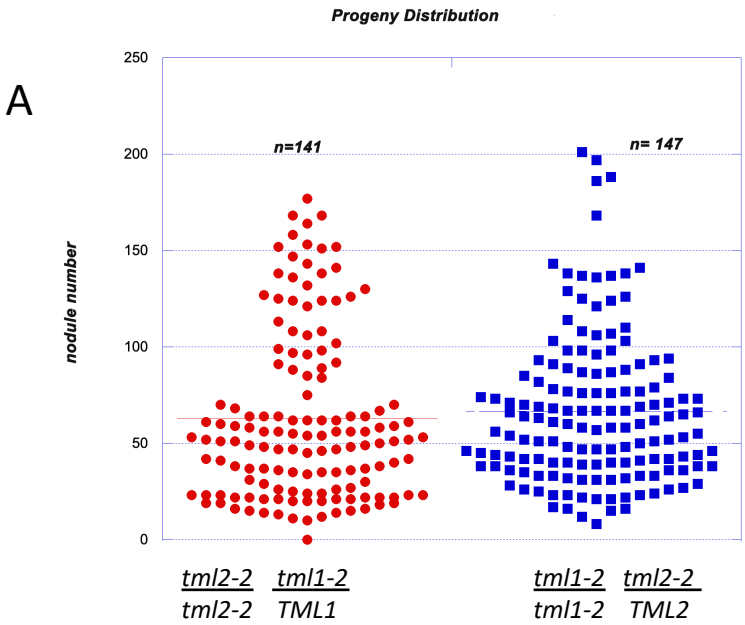

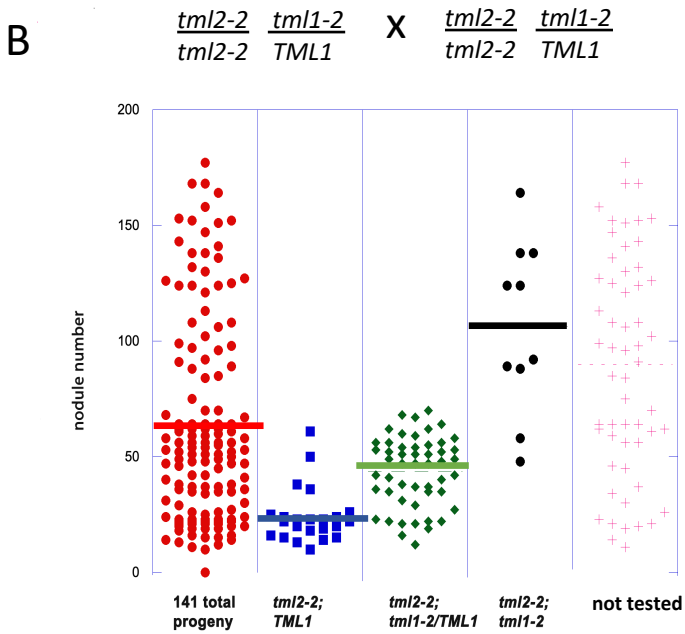

Figure 6. Distribution of nodulation number phenotypes demonstrates heterozygous effect. (A) Distribution plots of two populations of progeny from selfing of plant on X axis. Red dots are individual plant nodules numbers from *tml2-2* mutant plants segregating one wild type *TML1* allele, blue squares are *tml1-2* mutants segregating one wild type *TML2* allele. (B) *TML1* segregating population from A (red dots in both plots) broken down by molecular genotype. Blue are homozygous wild type *TML1,* green are heterozygous *tml1/TML1* and black are homozygous *tml1/tml1*. Lines indicate median nodule number for each group. A representative photo of plant phenotypes appears in Supplemental Figure 3.

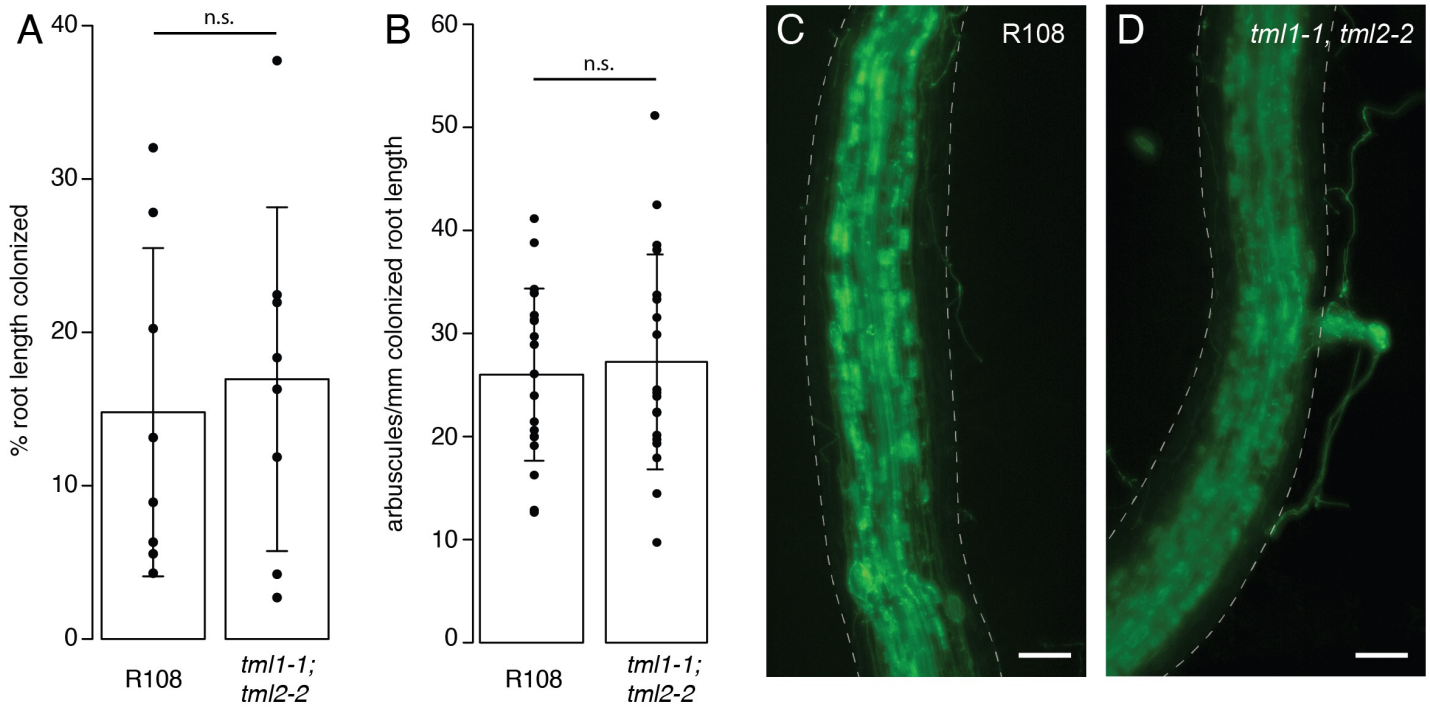

Figure 7. Arbuscular mycorrhiza symbiosis is not impaired in *tml1-1, tml2-2* double mutants. A) Overall root length colonization is similar in *tml1-1; tml2-2* double mutants and R108 wild-types. Student's t-test p>0.05 (not significant, n.s.). B) Arbuscule density (defined as arbuscules per mm of colonized root length) is not changed in *tml1-1; tml2-2* double mutants relative to R108 wild-type. Student's t-test p>0.05 (not significant, n.s.). C) Representative image of *Rhizophagus irregularis* symbiotic structures in an R108 wild-type root. D) Representative image of a *R. irregularis*-colonized root of a *tml1-1 tml2-2* double mutant. C, D) *R. irregularis* fungal structures are visualized with WGA-Alexafluor488. *M. truncatula* root is outlined with a dashed line. Scale bar: 100µm.

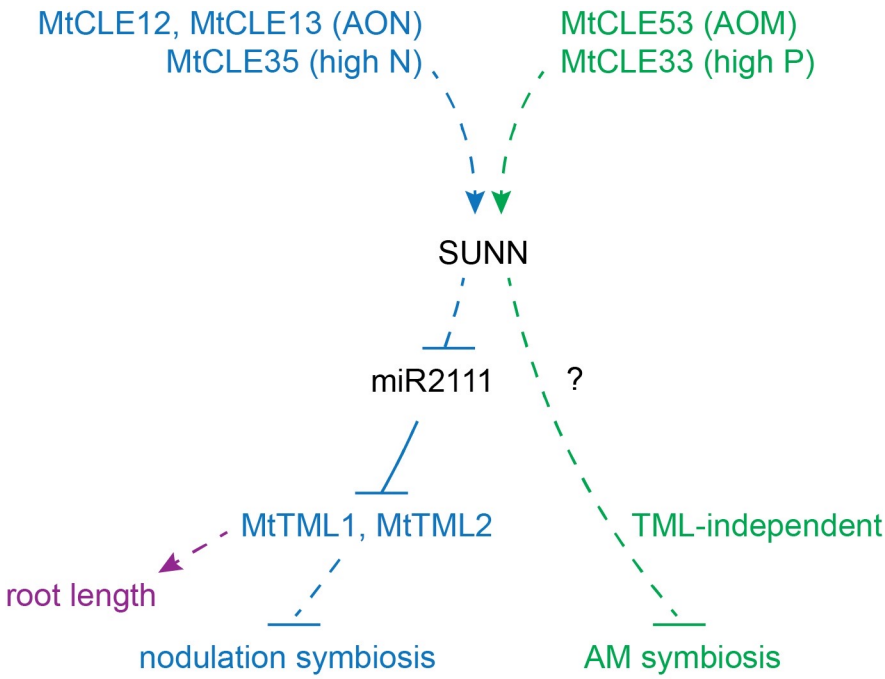

Figure 8. Model for Autoregulation Signaling in symbiosisFigure 8. Model for Autoregulation Signaling in symbiosis. Both rhizobial symbiosis (blue) and arbuscular mycorrhizal symbiosis (green) auto- and nutrient-regulation signal through the SUNN receptor kinase, but the presumed CLE peptide ligands for SUNN are different, and the data suggest that autoregulation downstream of SUNN bifurcates. See discussion for details.